Calvin Alexandre Fracassi Farias

Out-of-Equilibrium Statistical Mechanics Applied to Two-Dimensional Fluids

Mecânica Estatística Fora de Equilíbrio Aplicada a Fluidos Bidimensionais

Porto Alegre, Rio Grande do Sul
December, 2022

Calvin Alexandre Fracassi Farias

Out-of-Equilibrium Statistical Mechanics Applied to Two-Dimensional Fluids

Doctoral Thesis elaborated under the supervision of Prof. Yan Levin, co-supervision of Prof. Renato Pakter and presented to the Institute of Physics at UFRGS in partial fulfillment of the requirements for obtaining the title of Doctor in Physics.

Universidade Federal do Rio Grande do Sul – UFRGS
Instituto de Física
Graduate Program in Physics

Supervisor: Yan Levin
Co-supervisor: Renato Pakter

Porto Alegre, Rio Grande do Sul
December, 2022

There are many people to whom I should express my gratitude in different ways. Two out of many are particularly deserving. Without my parents, I could not even begin this.

From now on, everything is dedicated to them.

Acknowledgements

I will be brief with the acknowledgments. These last four years were quite different from the master's and undergraduate years in several ways. Completing the doctorate was an arduous learning task that was only possible given the work dynamics established with my advisors, Yan Levin and Renato Pakter. They were always available to me when I asked them, and sometimes when I did not ask them. Of course, there are other people who have supported me during this period, but in ways not directly related to the research. As far as this work is concerned, I reserve acknowledgement only for these two people.

Abstract

Systems whose components interact through long-range forces, such as self-gravitational systems and non-neutral plasmas, exhibit some intriguing properties compared to systems with screened or short-range forces. These systems evolve from perturbed states to long-lived transient states, often referred to as quasi-stationary states, and reach equilibrium only under certain conditions and on a very long time scale. Although technically there is no equilibrium, in many cases the behavior of quasi-stationary states can be described with a few macroscopic variables, suggesting a statistical approach. However, the tools of equilibrium statistical mechanics are not suitable for dealing with systems with long-range interactions. Not only do such systems exhibit special thermodynamic properties, such as negative specific heat and ensemble inequality, but their dynamics are predominantly non-collisional. Therefore, the dynamical properties must also be taken into account. In this thesis, we investigate these phenomena using theoretical models and numerical simulations. In particular, we use Kirchhoff's vortex formulation for two-dimensional Euler fluids to study the equilibrium state into which a two-dimensional incompressible fluid relaxes from an arbitrary initial flow. Employing Lynden-Bell relaxation theory, we then developed a method to find the state of maximum entropy of the fluid while preserving all Casimir invariants. We then approach quasi-stationary states by further developing the method to include the core-halo model with excellent results.

Key-words: long-range interacting systems; Vlasov dynamics; vortex fluids; Kirchhoff vortex; coherent structures.

Resumo

Sistemas cujos constituintes interagem através de forças de longo alcance, como sistemas auto-gravitacionais e plasmas não neutros, exibem algumas propriedades intrigantes em comparação com sistemas com forças blindadas ou de curto alcance. Esses sistemas evoluem de estados perturbados para estados transitórios de longa duração, geralmente chamados de estados quase-estacionários, e atingem o equilíbrio apenas sob certas condições e em uma escala de tempo muito longa. Embora tecnicamente não haja equilíbrio, em muitos casos o comportamento de estados quase estacionários pode ser descrito com algumas poucas variáveis macroscópicas, sugerindo uma abordagem estatística. No entanto, as ferramentas da mecânica estatística de equilíbrio não são adequadas para lidar com sistemas com interações de longo alcance. Tais sistemas não apenas exibem propriedades termodinâmicas especiais, como calor específico negativo e desigualdade de conjunto, mas sua dinâmica é predominantemente não colisional. Portanto, as propriedades dinâmicas também devem ser levadas em consideração. Nesta tese, investigamos esses fenômenos usando modelos teóricos e simulações numéricas. Em particular, usamos a formulação de vórtices de Kirchhoff para fluidos de Euler em duas dimensões para estudar o estado de equilíbrio no qual um fluido incompressível bidimensional relaxa a partir de um condição inicial arbitrária. Empregando a teoria de relaxamento de Lynden-Bell, desenvolvemos então um método para encontrar o estado de entropia máxima do fluido preservando todos os invariantes de Casimir. Em seguida, abordamos estados quase estacionários desenvolvendo ainda mais o método para incluir o modelo core-halo com excelentes resultados.

Palavras-chave: sistemas com interações de longo-alcance; dinâmica de Vlasov; fluidos de vórtices; vórtice de Kirchhoff; estruturas coerentes.

Simplified Abstract

Vortex fluids are a phenomenon belonging to a class of physical systems that exhibit several features that cannot be well explained by traditional statistical mechanics, such as the formation of large and coherent structures through an inverse process of energy transfer. Two good examples of coherent structures are Jupiter's famous red spot – a storm that has existed for at least three hundred years in an extremely violent environment – and elliptical galaxies such as the Milky Way. Other examples of vortices that have a greater impact on our daily lives include swirling currents in turbines (which can affect air travel), ocean eddies (which can affect shipping), and tornadoes (which are potentially capable of destroying infrastructure on a large scale and occasionally even claiming human lives).

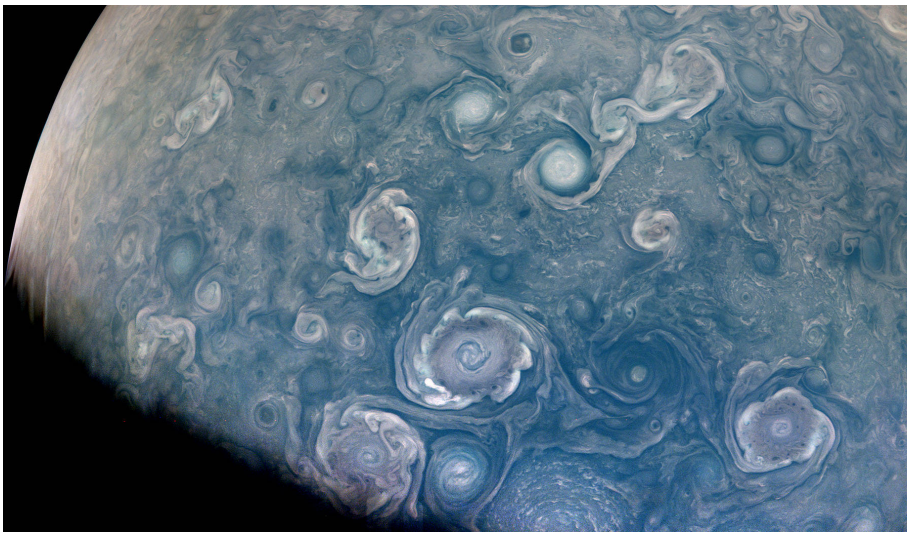

Figure 1 – NASA's Juno Mission picture of vortices near Jupiter's north pole. Image data from NASA/JPL-Caltech/SwRI/MSSS made available for public access.

In recent years, the study of vortices in fluids has again become an active field (Arnold and Khesin, Marchioro and Pulvirenti, Newton), but there are still open problems. Statistical methods and computer simulations are the usual tools to study these systems. Therefore, in this work we study the evolution of a certain type of vortex dynamics using these two methods, but we also present a newly developed tool for determining the final state of vortices that can be found from an arbitrary initial flow. The results obtained are very satisfactory and are based on the core-halo theory, which divides the vortex into a very dense central region and a thin halo in which the vortices are non-stationary.

CALVIN A FRACASSI FARIAS, **Out-of-Equilibrium Statistical Mechanics Applied to Two-Dimensional Fluids**. Thesis (Doctorate) – Instituto de Física, Universidade Federal do Rio Grande do Sul, Porto Alegre, 2022.

List of abbreviations and acronyms

CH	core-halo
LB	Lynden-Bell
LR	long-range
MD	molecular dynamics
qSS	*quasi*-stationary state

Contents

1 Introduction

The primary goal of statistical mechanics is to derive macroscopic properties from the microscopic structure of matter. In other words, it deals with the behavior of large systems consisting of a large number of particles, where the individual behavior of each particle cannot be predicted. It is an essential tool in many areas of physics, including condensed matter physics, nuclear physics, and astrophysics. Probabilistic properties are at the origin of statistical mechanics through the concept of statistical ensembles, an idealization that replicates the system under study in all its accessible microscopic states, each of which represents a possible state in which the real system might be. It is based on the assumption that the state of a system at a given time can be described by a probability distribution – for example, one might imagine that the particles in the system are subject to thermal fluctuations that allow the system to fluctuate rapidly among the many accessible microstates, so that the time-averaged measurement on the real system corresponds to an averaging of the property in the ensemble of microstates; thus, various macroscopic quantities such as the average energy or the average velocity of the particles can be calculated from this distribution without taking into account the microscopic dynamics. Not surprisingly, the fundamental postulate of statistical mechanics – *The Postulate of Equal A Priori Probabilities* – states that for an isolated system in thermodynamic equilibrium, the probability of reaching each of its accessible microscopic states must be the same [29]. For this reason, numerous conditions must be satisfied before classical statistical mechanics can be applied, such as ergodicity and mixing – an ergodic flow implies that there is a unique stationary probability density with a fixed energy at equilibrium that can be reached. However, there is no guarantee that such an equilibrium state will be reached unless it already starts there or at least there is the additional property of mixing [49]. For these and other reasons, classical statistical mechanics is a theory of matter in equilibrium. And although it is very successful in many areas of physics, there is a whole class of systems for which the necessary conditions are not satisfied.

In this thesis we are concerned with the special class of systems that interacts via long-range forces (LR). Typically, the pairwise potential $\phi(r)$ that characterizes a LR interaction is one that decays with exponents smaller than the dimensionality d of the embedding space [14], i.e., $\phi(r) \propto 1/r^{\gamma}$, where r is the distance in the configuration space and γ is any positive real number satisfying the condition $\gamma < d$. Examples include gravitation and electromagnetism, both topics that are well covered in undergraduate courses, but seldom in the context of statistical mechanics. One of the reasons for this is that in most systems treated by classical statistical mechanics, the transition time from a perturbed out-of-equilibrium state to a thermodynamic equilibrium state is very short compared to macroscopic observation times [12]. This is not true for LR interacting

systems, where collective effects occur due to particles interacting over large distances, leading to relaxation times that often diverge with the number of particles. These long-lived non-equilibrium transient states are called quasi-stationary states (qSS) [14, 56].

The most important condition for a short relaxation time is undoubtedly additivity. It refers to short-range interacting systems, where the interaction between their constituents decreases very rapidly with distance, so that the particles are able to thermalize "locally". The short-range nature of the forces also means that the interaction energy between two contacting systems comes from the surface layers in the contact region, whose thickness is on the order of the molecular length scale. This means that the total interaction energy between the two systems is due solely to the energy of their interface and becomes negligible as the size of the system increases. Moreover, it has been formally demonstrated that the property of additivity is responsible for the concavity of the thermodynamic potentials of entropy and free energy [50]. Therefore, the free energy and other thermodynamic functions of a non-additive composite system are not necessarily the sum of the corresponding quantities of its subsystems.

Since it is known that a system with long-range forces does not satisfy the additivity condition, the question arises to what extent classical statistical mechanics is applicable to these systems. It is now well known that non-additivity does not preclude a formal treatment of statistical mechanics, even though it leads to some results that may seem strange at first glance, such as inequivalence of ensembles [5, 32, 18], negative specific heat [53, 38, 9], and ergodicity breaking [48, 24, 31]. However, the absence of these properties has not prevented many attempts to apply equilibrium statistical mechanics to find steady states of systems with LR interactions [26, 43, 3, 7]. In particular, we observe two statistical approaches to systems whose potentials are long-ranged: i) Lynden-Bell's (LB) *violent relaxation* theory for computing the steady states of self-gravitating systems (SGS), where the violently changing gravitational field of newly formed galaxies plays an important role in the statistics of stellar orbits; and ii) Onsager's work on statistical hydrodynamics explaining the spontaneous formation of large-scale, long-lived vortices in two-dimensional flows as a consequence of equilibrium statistical mechanics at negative absolute temperature.

In a seminal work [37], Lynden-Bell observed the profile of galaxies and globular clusters and determined that there must be a similar relaxation process in all of them. LB then proposed a statistical theory to describe the steady state based on the conservation of density of the distribution function in the framework of Vlasov's dynamics. Under the assumption of collisionless dynamics, his theory accurately describes the steady state of initial distributions satisfying the virial condition. It is now known that a perturbed system, instead of immediately reaching thermodynamic equilibrium, first relaxes to a qSS with a characteristic time of order $\tau_v = O(1)$ by the process of violent relaxation. It is shown that the qSS is indeed a stationary state of the Vlasov equation. If the number

N of particles composing the system is finite, the system relaxes by finite size effects into a thermodynamic equilibrium state with a characteristic time of order $\tau_c = O(N^\zeta)$. The value of the exponent ζ is arguable, but for homogeneous water bag distributions it has been shown to be close to $\zeta \approx 1.7$ [56, 42].

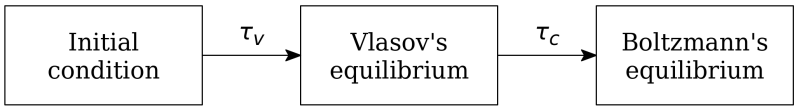

Figure 2 – Schematic description of the dynamical evolution of systems with LR interactions. First there is a violent relaxation at characteristic time $\tau_v = O(1)$, and then there is a collisional relaxation at characteristic time $\tau_c = O(N^\zeta)$.

The existence of qSS and the division of the relaxation process into two different time scales is due to the collisionless nature of the dynamics of LR interacting systems. The force acting on a particle of a many-body system is the result of its interaction with all other particles of the system. If these interactions do not decrease rapidly with distance, as in the case of a short-range interaction, the mean field is much more important to the dynamics of the particle than the interactions with its neighbors. At the thermodynamic limit, when $N \to \infty$, the dynamics is completely dominated by the mean field, and the particles move as if there were no collisions. In collisionless dynamics, the distribution function evolves like the density of an incompressible fluid. Thus, the local density remains constant along the flow while the distribution evolves. As a result, the distribution function undergoes a filamentation process on smaller and smaller length scales until finally the evolution takes place on such a small length scale that it is no longer perceptible to any observer. In this situation, a macroscopic (or coarse-grained) steady state of LB's statistics is reached while the underlying microscopic distribution function continues to evolve.

Similar to self-gravitating systems in which galaxies follow a type of organization revealed in the Hubble classification [8], hydrodynamic vortices, whose dynamics are governed by the Euler equation, occur in a variety of phenomena and show the formation of large-scale coherent structures in two-dimensional flows. The most remarkable feature of these coherent structures is their persistence in highly turbulent environments. For example, the Great Red Spot on Jupiter, a giant vortex that has persisted in turbulent shear for more than three centuries, is probably due to this general feature [40]. Just as the regularity in the light distribution of elliptical galaxies suggests a fundamental relaxation process, the spontaneous order observed in large-scale two-dimensional vortices suggests that there is an underlying principle governing the inverse energy cascade [44, 16]. In the case of two-dimensional turbulence, Onsager [46] was the first to suggest that an explanation might be found in the statistical mechanics of the Euler equations. In particular, he

showed that the state of maximum entropy has a negative absolute temperature when the vortices are considered as particles and Boltzmann statistical mechanics is invoked. The reason for such an inverted population is that, unlike particle systems, for fluids confined in a finite region – such as a planetary surface – the accessible phase space has a finite volume. The compact phase space leads to the fact that the entropy has two branches: one, in which it increases with the energy, similarly as in normal particle systems, and a branch, in which the entropy decreases with the energy. This second branch leads to a negative absolute temperature if the usual rules of thermodynamics are applied to define temperature. Ultimately, the presence of a negative temperature state would lead to a population inversion in which microscopic vortices cluster together to form a very small number of macroscopic vortices. In practice, a fluid need not be confined in a finite space to satisfy the conditions for the existence of a negative temperature state – conservation of angular momentum leads to an effective confinement potential, which also leads to self-confinement and population inversion [47].

Both Lynden-Bell's and Onsager's theories presuppose ergodicity and mixing, on which the thermodynamic argument is based. However, if Onsager's argument is correct, any uniform two-dimensional vortex distribution would have to relax into a huge circular vortex. On the other hand, it is known from the work of Kirchhoff that a uniform elliptical vortex undergoes rigid rotation and maintains its shape [30]. Moreover, it has recently been shown that a Kirchhoff vortex relaxes to a core-halo structure upon perturbation [47], which is very different from the circular vortex predicted by the Onsager theory of equilibrium statistical mechanics. The analogy between the violent relaxation and the mixing of vortices lies in the similar morphology of the Euler and Vlasov equations. And, as with SGS, there is an additional subtlety in the application of statistical mechanics to fluid dynamics. It is well known that the Euler equations for an incompressible two-dimensional fluid medium can be written in terms of vorticity. However, the vorticity Γ_i of the ith individual vortex must be infinitesimal, so that in the thermodynamic limit, when $N \to \infty$, the net vorticity remains finite and equal to $\sum_i^N \Gamma_i = \Gamma_T$. This is precisely the thermodynamic limit for systems with LR interactions in which the Vlasov equation governs the dynamics.

The core-halo model is not a complete theory as far as violent relaxation to quasi-stationary states is concerned, but it is undoubtedly relevant [25]. For example, it semi-quantitatively describes the relaxation of the Kirchhoff vortex to *quasi*-stationary states in a way that corresponds to the violent relaxation of self-gravitating systems. In this case however, unlike real particles, single point-like vortices of finite strength are physically impossible due to the infinite fluid velocity in the vortex core. Only vortices of infinitesimal strength are physically relevant, and indeed the Euler equation can only be mapped to a system with an infinite number of infinitesimal vortices. Unlike gravitational systems or plasmas, where collisional effects eventually lead to thermodynamic equilibrium after

a relaxation time that scales with the number of particles, this is not the case for fluid systems – the Euler fluid can only relax to a nonequilibrium steady state. For this reason the qSS is the last stage of evolution and is also called steady state.

In summary, stationary solutions of the Vlasov equation are transient states different from the Maxwell-Boltzmann equilibrium. They are not necessarily described by conventional thermodynamics and statistical mechanics, so dynamical aspects have to be considered and new tools have to be developed. In general, out-of-equilibrium steady states of LR interacting systems exhibit fascinating properties and are much more interesting than conventional thermodynamic equilibrium states. In recent years, a major effort has been made to incorporate these properties into an extended theory of the statistical mechanics of long-range interactions [14, 19, 35]. In the following, we will review the well-known theory on statistical approaches to these systems and present new, recently developed, investigation methods that focus on two-dimensional vortex dynamics. This thesis is organized as follows. In Chapter 2, we discuss the dynamical and equilibrium properties of systems with long-range interactions, examining some key properties such as non-additivity, inequivalence of statistical ensembles, reduced distribution functions and collisionless dynamics. In Chapter 2 we discuss some aspects of Lynden-Bell's violent relaxation and the principle of maximum entropy, and in Subsection 3.2.2 we present an algorithm for automatically finding the configuration that maximizes entropy. Finally, two-dimensional incompressible fluid dynamics and molecular dynamics simulations are discussed in Chapter 4, and a newly developed stochastic method based on the core-halo model is discussed in Section 4.3.

Part I

Literature review

2 Dynamical and Equilibrium Properties of Long-Range Interactions

The large number of particles in many-body systems is one of the reasons why statistical mechanics is one of the most successful theories in physics. Even with a large number of degrees of freedom, the equilibrium state reached by a many-body system usually depends only on external thermodynamic parameters, such as volume and temperature, allowing one to approach it using the concept of statistical ensembles. However, long-range interacting systems exhibit transient states with longstanding lifetimes that may diverge in the thermodynamic limit. Yet, the tools of statistical mechanics do not provide information about the transient states or the time scale on which the process occurs, such that one must resort to kinetic theories to study out-of-equilibrium dynamics, especially the approach to *quasi*-stationary states.

In this chapter, we revisit statistical equilibrium properties of long-range interactive systems and also their dynamical properties – in particular, the derivation of the Boltzmann transport equation and kinetic theories such as the one-particle distribution function.

2.1 Non-additivity and the Definition of Long-Range Interactions

Systems with long-range interactions differ from systems with short-range interactions mainly by the contributions to their internal energy, since the interactions between different subsystems cannot be neglected. Long-range interactions is a definition of systems whose pairwise interacting potential decays slowly. For example, consider the particular case where the interaction potential $\phi(r)$ is equal to

$$\phi(r) = \frac{\kappa}{r^\gamma}, \tag{2.1}$$

where κ is a coupling constant, r is the distance in the configuration space, and γ is an arbitrary scalar number that controls the range of the interaction. Let the internal energy U of a particle located in the center of a d-dimensional (hyper-)sphere of radius R filled with homogeneous density ρ be equal to

$$U = \int_\delta^R \frac{\rho\,\kappa}{r^\gamma}\,\mathrm{d}^d r \tag{2.2}$$

where δ is an arbitrarily small radius for which the contributions from within are neglected. At the increasing limit of the sphere radius R and with δ tending to zero, the energy remains finite only if γ is larger than d. Otherwise, the energy increases linearly with the

volume size, $V \propto R^d$, diverging in the limit $R \to \infty$, as shown below.

$$U = \rho\,\kappa\,\Omega_d \int_\delta^R r^{d-1-\gamma}\,\mathrm{d}r = \frac{\rho\,\kappa\,\Omega_d}{d-\gamma}\left[R^{d-\gamma} - \delta^{d-\gamma}\right], \qquad \text{if } d \neq \gamma. \tag{2.3}$$

Here, Ω_d is the angular volume of a d-dimensional (hyper-)sphere. In the limiting case, where $d = \gamma$, the argument is preserved, but the expression diverges logarithmically. For this reason, LR interacting systems are also called *non-integrable*. Moreover, it can be generalized that for LR interactions each particle interacts with every other particle, so that the interaction energy grows superlinearly with the number of particles. As a result, LRI systems are not expected to be either additive or extensive.

The state of thermodynamic equilibrium can be fully specified by a few parameters, called state variables, which must be either extensive or intensive [12, 49]. An extensive state variable is defined as a variable whose magnitude is additive for its subsystems, e.g., the internal energy U of a system composed of N particles is extensive if for an arbitrary scalar λ, the equality $U(\lambda N) = \lambda U(N)$ is satisfied. However, the example above has shown that this is not the case under the framework of long-range interactions.

Extensivity can be recovered by redefining the coupling constant $\kappa' \to \kappa V^{\sigma/d-1}$, where V represents the volume of the system. In particular, the Kac's prescription corresponds to the case where $\sigma = 0$, and it's usually applied for mean-field models in the form of an $1/N$ prefactor [10].

The two concepts of additivity and extensivity are related but different. To illustrate this difference, consider the Curie-Weiss-Hamiltonian mean-field, an over-simplification of the Ising model:

$$H_{CW} = \frac{-\kappa}{2N}\sum_{i=1}^{N}\sum_{j=1}^{N} s_i s_j = \frac{-\kappa}{2N}\left(\sum_{i=1}^{N} s_i\right)^2, \tag{2.4}$$

where there are no external magnetic field and the spins variables may assume the values $s_i = \pm 1$. In this system the distance does not matter, the spins are equally influenced by all other spins. Then, the prefactor $1/N$ in (2.4) guarantees the convergence of the energy per particle to a finite value in the thermodynamic limit. Note that doubling the number N of spins also doubles the energy, which proves that it is an extensive quantity. However, the Hamiltonian is not additive. One can imagine that the system is divided into two equal parts, where on one part all spins have the sign $+1$ and on the other part all spins have the sign -1. The energy of each part is thus evaluated as $E_1 = E_2 = -\kappa N/4$, but the total energy of the whole system is clearly $E_{total} = 0$. So it is thus established that the Curie-Weiss-Hamiltonian mean field is extensive but not additive.

The absence of additivity leads to all the peculiar properties of systems with long-range interactions. Among these properties is the negative specific heat in the microcanonical ensemble, which results from the fact that entropy may exhibit non-concave intervals in the absence of additivity. In fact, it is the additivity property that guarantees the

concavity of the entropy [50]. And since negative specific heat is not possible in the canonical ensemble, the long-range interactions also lead to the possibility of inequality of statistical ensembles.

2.2 Ensemble Inequivalence and Negative Specific Heat

In statistical mechanics, the concept of nonequivalence of ensembles refers to the fact that different statistical ensembles used to describe the behavior of a system in thermodynamic equilibrium may give different predictions for the macroscopic properties of the system. This may be the case because the ensembles are based on different assumptions about the constraints imposed on the system.

One way to understand the nonequivalence of ensembles is to consider the concept of convexity. A convex function always lies above its tangent lines, while a concave function lies below its tangent lines. The convex envelope of a function is the function obtained by taking the lower envelope of all tangents to the original function. Therefore, a thermodynamic function is said to be convex if it contains all the line segments connecting any two pairs of points. In general, a limited part of the available space is accessible to the system, which is due to the specifics of the system under study. However, the accessible part is always convex when short range interactions are involved, which is a direct consequence of additivity. If long-range interactions are at play, the lack of additivity can cause the associated spaces to be non-convex, even if there are convex regions – the so called convex intruders. Then, for example, the entropy may exhibit gaps in the domain of its thermodynamic parameters that prevent the system from moving into other valid domains, which means that the intermediate values of the extensive parameters are not necessarily accessible and that the ergodicity condition is not satisfied [14, 50].

If concave domains are found in thermodynamic functions, such as the microcanonical entropy, Legendre transformation is not correct, yielding a *concave envelope* that ultimately leads to inequivalence between statistical ensembles. The physical consequences are many, but one of the most relevant for this work arises from the *concave envelope* of the entropy-energy curve, which causes a negative specific heat. The heat capacity at constant volume is defined as $C_v = \partial E/\partial T$. Therefore, the relation

$$\frac{\partial^2 S}{\partial E^2} = \frac{-1}{C_v T^2}, \tag{2.5}$$

implies that C_v is negative in the interval $[E_1, E_2]$ shown in Figure 3, since the convexity of the entropy $\partial^2 S/\partial E^2 > 0$ in the same interval.

The nonequivalence of ensembles arises from the fact that the predictions of the microcanonical and canonical ensembles may be different for the macroscopic properties of the system, even though both ensembles are based on the same underlying statistical mechanics. This is because the assumptions about the constraints imposed on the system

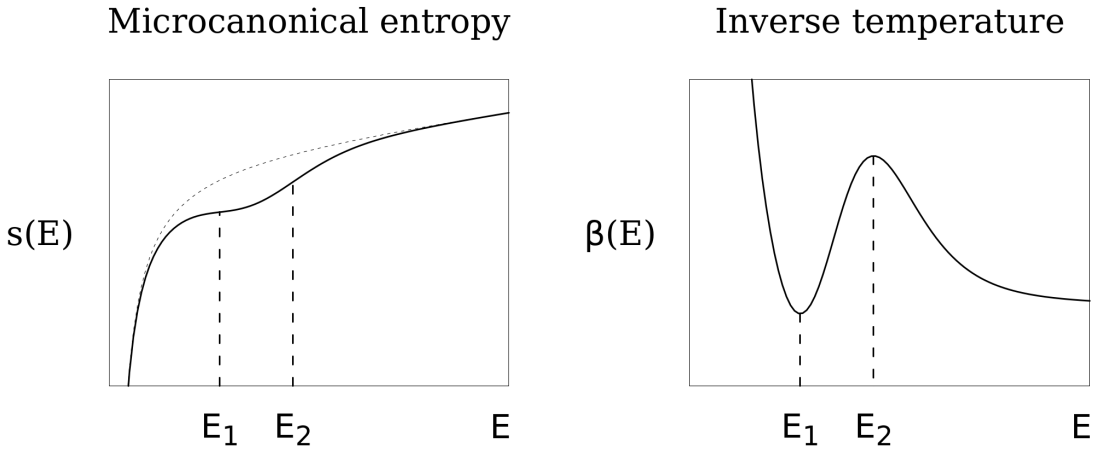

Figure 3 – Schematic representation of a fictitious thermodynamic function of the microcanonical entropy $s(E)$ exhibiting the *concave envelope* and the correspondent schematic representation of the inverse temperature $\beta(E)$. The dashed thin line in the left panel shows the entropy-energy curve if additivity were satisfied.

lead to different predictions for the behavior of the system as a whole. Negative specific heat is possible only in the microcanonical ensemble – in the canonical ensemble the specific heat is positive by definition. Therefore, near phase transitions, ensembles may be inequivalent [5, 52]. It turns out that first order phase transitions in the canonical ensemble are a necessary condition for the inequality of the ensembles.

2.3 Kinetic Theory and Reduced Distribution Functions

The solution of a kinetic equation determines the dynamic state of the distribution function of a single particle. Consequently, the kinetic equation must be a closed equation of the single-particle distribution function. The BBGKY hierarchy, an approach that takes into account the full N-body dynamics and was proposed almost simultaneously by Bogoliubov (1946), Born and Green (1949), Kirkwood (1946), and Yvon (1935), is often used in the derivation of the Boltzmann transport equation. It is as follows.

Consider a d-dimensional system composed of N identical particles of mass m. The Hamiltonian is written as

$$\mathscr{H} = \sum_{i=1}^{N} \frac{\boldsymbol{p}_i^2}{2m} + \frac{1}{2}\sum_{i=1}^{N}\sum_{j\neq i}^{N} V\big(|\boldsymbol{q}_i - \boldsymbol{q}_j|\big), \tag{2.6}$$

where $\boldsymbol{q}_i$ and $\boldsymbol{p}_i$ are respectively the coordinates of position and conjugate momenta of the ith particle. The particles interact with each other by the central potential $V\big(|\boldsymbol{q}_i - \boldsymbol{q}_j|\big)$, or V_{ij} for short. The full N-body distribution function $f^{(N)}(\boldsymbol{x}_1, \ldots, \boldsymbol{x}_N, t)$ accurately describes the evolution of the system in a $2dN$-dimensional phase space, where $\boldsymbol{x}_i$ is defined as the $2d$-dimensional vector $(\boldsymbol{q}_i, \boldsymbol{p}_i)$. The probability of encountering the system

at a time t in the infinitesimal volume $\mathrm{d}\boldsymbol{x}_1 \ldots \mathrm{d}\boldsymbol{x}_N$ around the phase space coordinate $(\boldsymbol{x}_1, \ldots, \boldsymbol{x}_N)$ is thus proportional to $f^{(N)}(\boldsymbol{x}_1, \ldots, \boldsymbol{x}_N, t)\,\mathrm{d}\boldsymbol{x}_1 \ldots \mathrm{d}\boldsymbol{x}_N$. Since the probability that the system is somewhere in the phase space is equal to one at any time, the evolution of the distribution function is determined by the continuity equation, i.e.,

$$\frac{\partial}{\partial t} f^{(N)}(\{\boldsymbol{x}_i\}, t) + \sum_{j=1}^{N} \frac{\partial}{\partial \boldsymbol{x}_j}\Big(\dot{\boldsymbol{x}}_j \cdot f^{(N)}(\{\boldsymbol{x}_i\}, t)\Big) = 0 \tag{2.7}$$

where $\{\boldsymbol{x}_i\}$ denotes the set of vectors $\boldsymbol{x}_i \; \forall\, i \in \{1, \ldots, N\}$. If the coordinate and momentum variables are put in evidence, the continuity equation is written as follows.

$$\begin{aligned} &\frac{\partial}{\partial t} f^{(N)}(\{\boldsymbol{q}_i\}, \{\boldsymbol{p}_i\}, t) + \sum_{j=1}^{N} \dot{\boldsymbol{q}}_i \cdot \boldsymbol{\nabla}_j f^{(N)}(\{\boldsymbol{q}_i\}, \{\boldsymbol{p}_i\}, t) \\ &\quad + \sum_{j=1}^{N} \dot{\boldsymbol{p}}_j \cdot \frac{\partial}{\partial \boldsymbol{p}_j} f^{(N)}(\{\boldsymbol{q}_i\}, \{\boldsymbol{p}_i\}, t) = 0 \end{aligned} \tag{2.8}$$

where the usual notation $\boldsymbol{\nabla}_i \equiv \partial/\partial \boldsymbol{q}_i$ was adopted. Once the Hamiltonian's equations of motion,

$$\dot{\boldsymbol{q}}_i = \frac{\boldsymbol{p}_i}{m}, \tag{2.9}$$

$$\dot{\boldsymbol{p}}_i = -\sum_{j \neq i}^{N} (\boldsymbol{\nabla}_i V_{ij}), \tag{2.10}$$

are introduced, the Liouville equation is obtained:

$$\begin{aligned} &\frac{\partial}{\partial t} f^{(N)}(\{\boldsymbol{q}_i\}, \{\boldsymbol{p}_i\}, t) + \sum_{i=1}^{N} \frac{\boldsymbol{p}_i}{m} \cdot \boldsymbol{\nabla}_i f^{(N)}(\{\boldsymbol{q}_i\}, \{\boldsymbol{p}_i\}, t) \\ &\quad - \sum_{i=1}^{N} \sum_{j \neq i}^{N} (\boldsymbol{\nabla}_i V_{ij}) \cdot \frac{\partial}{\partial \boldsymbol{p}_i} f^{(N)}(\{\boldsymbol{q}_i\}, \{\boldsymbol{p}_i\}, t) = 0. \end{aligned} \tag{2.11}$$

However, it is challenging to deal with Liouville's equation of $f^{(N)}(\{\boldsymbol{q}_i\}, \{\boldsymbol{p}_i\}, t)$ since it describes the evolution of a $2dN$-dimensional function. To simplify this treatment, we can define reduced distribution functions by integrating over some degrees of freedom. In particular, the reduced s-particle distribution function is defined by the partial integration of the N-body distribution function, i.e.,

$$f^{(s)}(\boldsymbol{x}_1, \ldots, \boldsymbol{x}_s, t) = \frac{N!}{(N-s)!} \int \mathrm{d}\boldsymbol{x}_{s+1} \ldots \mathrm{d}\boldsymbol{x}_N \, f^{(N)}(\boldsymbol{x}_1, \ldots, \boldsymbol{x}_N, t). \tag{2.12}$$

Since both Hamilton's equation and Liouville's equation are invariant to the permutation of any two particles, the distribution function must also satisfy this condition. Thus, there is no dilemma concerning the question which set of $(N-s)$ particles should be integrated in order to obtain the reduced s-particle distribution function. If we further assume that the distribution function $f^{(N)}(\{\boldsymbol{x}_i\}, t)$ is normalized to unity, then $f^{(s)}(\boldsymbol{x}_1, \ldots, \boldsymbol{x}_s, t)$ is normalized to

$$\int \mathrm{d}\boldsymbol{x}_1 \ldots \mathrm{d}\boldsymbol{x}_s \; f^{(s)}(\boldsymbol{x}_1, \ldots, \boldsymbol{x}_s, t) = \frac{N!}{(N-s)!}. \tag{2.13}$$

The time evolution of the s-particle distribution function can be calculated by the corresponding partial integration of the Liouville equation. If one then assumes that $f^{(N)}(\{\boldsymbol{x}_i\}, t)$ vanishes at the boundary domain of definition, i.e.,

$$\int \mathrm{d}\boldsymbol{x}_i \, \frac{\boldsymbol{p}_i}{m} \cdot \boldsymbol{\nabla}_i f^{(N)}(\{\boldsymbol{x}_i\}, t) = 0 \qquad \text{and} \tag{2.14}$$

$$\int \mathrm{d}\boldsymbol{x}_i \, (\boldsymbol{\nabla}_i V_{ij}) \cdot \frac{\partial}{\partial \boldsymbol{p}_i} f^{(N)}(\{\boldsymbol{x}_i\}, t) = 0, \tag{2.15}$$

the time evolution is given by

$$\begin{aligned} \frac{\partial}{\partial t} f^{(s)}(\boldsymbol{x}_1, \ldots, \boldsymbol{x}_s, t) &= -\sum_{i=1}^{s} \frac{\boldsymbol{p}_i}{m} \cdot \boldsymbol{\nabla}_i f^{(s)}(\boldsymbol{x}_1, \ldots, \boldsymbol{x}_s, t) \\ &+ \sum_{i=1}^{s} \sum_{j \neq i}^{s} (\boldsymbol{\nabla}_i V_{ij}) \cdot \frac{\partial}{\partial \boldsymbol{p}_i} f^{(s)}(\boldsymbol{x}_1, \ldots, \boldsymbol{x}_s, t) \\ &+ \sum_{i=1}^{s} \int \mathrm{d}\boldsymbol{x}_{s+1} \, (\boldsymbol{\nabla}_i V_{i,s+1}) \cdot \frac{\partial}{\partial \boldsymbol{p}_i} f^{(s+1)}(\boldsymbol{x}_1, \ldots, \boldsymbol{x}_s, t) \qquad \text{if } s \in \{2, \ldots, N-1\}. \end{aligned} \tag{2.16}$$

When $s = 1$, the above equation holds without the second term on the right-hand side. Together, the Liouville equation (2.11) and the above equation (2.16) form what is known as the BBGKY hierarchy: a set of N coupled integro-differential equations in which the time evolution of each distribution $f^{(s)}(\boldsymbol{x}_1, \ldots, \boldsymbol{x}_s, t)$ is coupled to the distribution $f^{(s+1)}(\boldsymbol{x}_1, \ldots, \boldsymbol{x}_{s+1}, t)$, except for the Liouville equation itself, which is a closed equation for $f^{(N)}(\{\boldsymbol{x}_i\}, t)$.

So far, the BBGKY hierarchy does not provide a closed equation for a reduced s-particle distribution function. However, it is expected that a truncation of the hierarchy to a small value of s by introducing some degree of approximation may be appropriate. For certain "families" of observables, knowledge of the first few distribution functions $f^{(s)}(\boldsymbol{x}_1, \ldots, \boldsymbol{x}_s, t)$, even if not exact, may be sufficient to compute the expected values of their observables. For example, suppose that an observable O is the sum of identical one-particle functions a,

$$O(\boldsymbol{x}_1, \ldots, \boldsymbol{x}_N) = \sum_{i=1}^{N} a(\boldsymbol{x}_i). \tag{2.17}$$

The expected value $\langle O \rangle$ is given by

$$\langle O \rangle(t) = \int \mathrm{d}\boldsymbol{x}_1 \ldots \mathrm{d}\boldsymbol{x}_N \; O(\boldsymbol{x}_1, \ldots, \boldsymbol{x}_N) \, f^{(N)}(\boldsymbol{x}_1, \ldots, \boldsymbol{x}_N, t) \tag{2.18}$$

$$= \int \mathrm{d}\boldsymbol{x}_1 \ldots \mathrm{d}\boldsymbol{x}_N \sum_{i=1}^{N} a(\boldsymbol{x}_i) \, f^{(N)}(\boldsymbol{x}_1, \ldots, \boldsymbol{x}_N, t). \tag{2.19}$$

Reducing to the one-particle distribution function, i.e., the particular case where $s = 1$ in (2.12), and recalling the conditions of normalization and permutation of the reduced

s-particle distribution function, the expected value $\langle O \rangle$ is given by

$$\begin{aligned}\langle O \rangle(t) &= \sum_{i=1}^{N} \Big(\int \mathrm{d}\boldsymbol{x}_i \; a(\boldsymbol{x}_i) \\ &\quad \times \int \mathrm{d}\boldsymbol{x}_1 \ldots \mathrm{d}\boldsymbol{x}_{i-1}\, \mathrm{d}\boldsymbol{x}_{i+1} \ldots \mathrm{d}\boldsymbol{x}_N \; f^{(N)}(\boldsymbol{x}_1, \ldots, \boldsymbol{x}_N, t) \Big) \qquad (2.20) \\ &= \sum_{i=1}^{N} \left(\int \mathrm{d}\boldsymbol{x}_i \; a(\boldsymbol{x}_i) \times \frac{(N-1)!}{N!} f^{(1)}(\boldsymbol{x}_i, t) \right) \qquad (2.21) \\ &= \int \mathrm{d}\boldsymbol{x}_1 \; a(\boldsymbol{x}_1) f^{(1)}(\boldsymbol{x}_1, t). \qquad (2.22)\end{aligned}$$

Although the expected value is written in terms of the one-particle distribution function, it still depends on $f^{(2)}(\boldsymbol{x}_1, \boldsymbol{x}_2, t)$, which depends on $f^{(3)}(\boldsymbol{x}_1, \boldsymbol{x}_2, \boldsymbol{x}_3, t)$, and so on. To establish a closed equation for $f^{(1)}(\boldsymbol{x}_1, t)$, or $f^{(2)}(\boldsymbol{x}_1, \boldsymbol{x}_2, t)$ for what matters, additional approximations are required, but these depend on the nature of the system under consideration. A general expression that facilitates additional approximations is to write

$$f^{(2)}(\boldsymbol{x}_1, \boldsymbol{x}_2, t) = f^{(1)}(\boldsymbol{x}_1, t)\, f^{(1)}(\boldsymbol{x}_2, t) + g^{(2)}(\boldsymbol{x}_1, \boldsymbol{x}_2, t) \qquad (2.23)$$

$$\begin{aligned}f^{(3)}(\boldsymbol{x}_1, \boldsymbol{x}_2, \boldsymbol{x}_3, t) &= f^{(1)}(\boldsymbol{x}_1, t) f^{(1)}(\boldsymbol{x}_2, t) f^{(1)}(\boldsymbol{x}_3, t) \\ &\quad + f^{(1)}(\boldsymbol{x}_1, t)\, g^{(2)}(\boldsymbol{x}_2, \boldsymbol{x}_3, t) + f^{(1)}(\boldsymbol{x}_2, t)\, g^{(2)}(\boldsymbol{x}_1, \boldsymbol{x}_3, t) \\ &\quad + f^{(1)}(\boldsymbol{x}_3, t)\, g^{(2)}(\boldsymbol{x}_1, \boldsymbol{x}_2, t) + g^{(3)}(\boldsymbol{x}_1, \boldsymbol{x}_2, \boldsymbol{x}_3, t)\end{aligned} \qquad (2.24)$$

where $g^{(s)}$, with $s = 2$ and $s = 3$ in the above equations, is the correlation function of the s-particle distribution function and refers to the deviation from the complete distribution function in its uncorrelated form. The time evolution of the one-particle distribution function is then written as follows,

$$\begin{aligned}&\frac{\partial}{\partial t} f^{(1)}(\boldsymbol{x}_1, t) + \frac{\boldsymbol{p}_1}{m} \cdot \boldsymbol{\nabla}_1 f^{(1)}(\boldsymbol{x}_1, t) - \Big(\boldsymbol{\nabla}_1 V\big[f^{(1)}, t\big] \Big) \cdot \frac{\partial}{\partial \boldsymbol{p}_1} f^{(1)}(\boldsymbol{x}_1, t) \\ &\qquad = \int \mathrm{d}\boldsymbol{x}_2 \, (\boldsymbol{\nabla}_1 V_{12}) \cdot \frac{\partial}{\partial \boldsymbol{p}_1} g^{(2)}(\boldsymbol{x}_1, \boldsymbol{x}_2, t),\end{aligned} \qquad (2.25)$$

where $V[f^{(1)}, t]$ is the averaged two-particle interaction potential:

$$V[f^{(1)}, t] = \int \mathrm{d}\boldsymbol{x}_2 \; V_{12} f^{(1)}(\boldsymbol{x}_2, t). \qquad (2.26)$$

The equation (2.25) shows that the effects of the interactions on the evolution of the one-particle distribution function can be divided into two terms. The last term on the left-hand side corresponds to a mean field potential, while the term on the right-hand side is a pairwise interaction potential that depends on the correlation function. For LR interactions, the range of the potential spans the entire system, and if it is not

homogeneous, the mean field dominates over the term with the correlation function, while for short-range interactions, the gradient of the mean field is negligible because the characteristic variation length of the potential is much smaller than that of the one-particle distribution function, while the correlation function and its gradient will have a similar range as the interaction potential. Therefore, for systems with short-range interactions, the term on the right-hand side dominates comparing to the mean field term. A common approximation is to set $g^{(2)}(\boldsymbol{x}_1, \boldsymbol{x}_2, t)$ to *zero* when at the thermodynamic limit, which is satisfactory for LR interacting systems for the reasons given above.

2.4 Deduction of the Vlasov Equation from the Klimontovich Equation

This section is devoted to the derivation of the Vlasov equation in a simpler procedure than the derivation from the BBGKY hierarchy. The derivations presented here are restricted to a one-dimensional system with periodic boundary conditions in the configuration space. However, they can be easily extended to two or three dimensions. The motivation behind the Vlasov equation, as we will see below, is to represent the qSS as an equilibrium state of the underlying continuum evolution of the distribution function.

Let the Hamiltonian of a system consisting of N particles be as follows.

$$\mathscr{H} = \sum_{j=1}^{N} \frac{P_j}{2} + U(\{\Theta_j\}) \tag{2.27}$$

where Θ_j and P_j are the canonical coordinates and momenta of the jth particle, respectively. Let the system be periodic in space with $\Theta_j \in [0, 2\pi)$ and the potential be a sum of pair interactions, such as

$$U(\Theta_1, \ldots, \Theta_N) = \frac{1}{2} \sum_{i=1}^{N} \sum_{j \neq i}^{N} V(\Theta_i - \Theta_j). \tag{2.28}$$

The discrete time-dependent density function of the above system is described by

$$f_d(\theta, p, t) = \frac{1}{N} \sum_{i=1}^{N} \delta(\theta - \Theta_j(t))\, \theta(p - P_j(t)) \tag{2.29}$$

where δ denotes the Dirac *delta* function and (θ, p) is the Eulerian coordinate in the phase space. By differentiating with respect to time, the density function takes the following form

$$\begin{aligned} \frac{\partial}{\partial t} f_d(\theta, p, t) = &-\frac{1}{N} \sum_{i=1}^{N} P_j \; \frac{\partial}{\partial \theta} \Big(\delta(\theta - \Theta_j(t))\, \delta(p - P_j(t)) \Big) \\ &+ \frac{1}{N} \sum_{i=1}^{N} \frac{\partial U}{\partial \Theta_j} \; \frac{\partial}{\partial p} \Big(\delta(\theta - \Theta_j(t))\, \delta(p - P_j(t)) \Big) . \end{aligned} \tag{2.30}$$

At this point Hamilton's equations of motion were introduced. Using the following property of the delta function: $a\delta(a-b) = b\delta(a-b)$, equation 2.30 can also, be written as

$$\begin{aligned}\frac{\partial}{\partial t} f_d(\theta, p, t) = &-\frac{1}{N}\sum_{i=1}^{N} p\ \frac{\partial}{\partial \theta}\Big(\,\delta(\theta - \Theta_j(t))\,\delta(p - P_j(t))\Big) \\ &+ \frac{1}{N}\sum_{i=1}^{N}\frac{\partial v}{\partial \theta}\ \frac{\partial}{\partial p}\Big(\,\delta(\theta - \Theta_j(t))\,\delta(p - P_j(t))\Big)\,,\end{aligned} \tag{2.31}$$

where

$$v(\theta, t) = N\int \mathrm{d}\theta'\,\mathrm{d}p'\,V(\theta - \theta') f_d(\theta', p', t). \tag{2.32}$$

After rearranging the terms, we obtain the formal expression for the Klimontovich equation. It is also important to note that this derivation is also exact for a finite number N of particles.

$$\frac{\partial f_d}{\partial t} + p\frac{\partial f_d}{\partial \theta} - \frac{\partial v}{\partial \theta}\frac{\partial f_d}{\partial p} = 0. \tag{2.33}$$

The Klimontovich equation is the equivalent of Hamilton's equations of motion, i.e., it contains the information about the orbit of each particle, which makes its solution very difficult, if not impractical, for a many-body system. Alternatively, starting from a well-defined set of initial conditions, all close to the same macroscopic state, one could define an averaged one-particle distribution function, called f_0, and performed over the density of such a macroscopic initial state, denominated $f_{in}(\{\Theta_i(0)\}, \{P_i(0)\}, t)$.

$$f_0(\theta, p, t) = \langle f_d(\theta, p, t)\rangle \tag{2.34}$$

$$= \int \prod_i \mathrm{d}\Theta_i(0)\,\mathrm{d}P_i(0)\, f_{in}(\{\Theta_i(0), P_i(0)\}) f_d(\theta, p, t). \tag{2.35}$$

Unlike equation (2.29), which is discrete, f_0 is smooth, and its time evolution is again given by an average over f_{in}. At this point, it should be noted that the fluctuations δf around the smooth distribution are defined as follows

$$f_d(\theta, p, t) = f_0(\theta, p, t) + \frac{1}{\sqrt{N}}\delta f(\theta, p, t) \tag{2.36}$$

The physical interpretation of the above equation is that after integrating the quantity δf, i.e., the difference between a singular distribution function containing Dirac delta functions and the smooth distribution function, over an area large enough to contain many particles but small compared to the total available space, its result will be of order $1/\sqrt{N}$. Thus, substituting the above equation (2.36) into equation (2.32), we obtain the following result

$$v(\theta, t) = \langle v\rangle(\theta, t) + \frac{1}{\sqrt{N}}\delta v(\theta, t) \tag{2.37}$$

where the first term is an average over f_{in} and the second defines δv. Substituting the last two expressions into the Klimontovich equation, we get

$$\begin{aligned}\frac{\partial f_0}{\partial t} + p\frac{\partial f_0}{\partial \theta} - \frac{\partial \langle v\rangle}{\partial \theta}\frac{\partial f_0}{\partial p} \\ = -\frac{1}{N}\left(\frac{\partial \delta f}{\partial t} + p\frac{\partial \delta f}{\partial \theta} - \frac{\partial \delta v}{\partial \theta}\frac{\partial f_0}{\partial p} - \frac{\partial \langle v\rangle}{\partial \theta}\frac{\partial \delta f}{\partial p}\right) + \frac{1}{N}\frac{\partial \delta v}{\partial \theta}\frac{\partial \delta f}{\partial p}.\end{aligned} \tag{2.38}$$

After averaging over f_{in} we get

$$\frac{\partial f_0}{\partial t} + p\frac{\partial f_0}{\partial \theta} - \frac{\partial \langle v\rangle}{\partial \theta}\frac{\partial f_0}{\partial p} = \frac{1}{N}\left\langle \frac{\partial \delta v}{\partial \theta}\frac{\partial \delta f}{\partial p}\right\rangle. \tag{2.39}$$

Any average over f_{in} by the terms containing δf or δv will be zero, since they depend on all Lagrangian variables of the initial state. Therefore, equation (2.39) is the equivalent of equation (2.25) and is an exact expression. The right-hand side of the equation usually corresponds to the collision term of the Boltzmann transport equation when short-range forces are acting. Since the right-hand side is of order $1/N$, it can be neglected at the thermodynamic limit, leading to the Vlasov equation

$$\frac{\partial f_0}{\partial t} + p\frac{\partial f_0}{\partial \theta} - \frac{\partial \langle v\rangle}{\partial \theta}\frac{\partial f_0}{\partial p} = 0. \tag{2.40}$$

Part II

Applications

3 Lynden-Bell's Maximum Entropy Principle

This chapter is devoted to the discussion of relaxation for *quasi*-stationary states of systems with long-range interactions according to the Lynden-Bell approach. The similarities of macroscopic systems, specifically the light distribution of elliptical galaxies, motivated Lynden-Bell to propose a theory of fast relaxation based on energy exchange through parametric resonances of the self-consistent mean field. Lynden-Bell referred to this process as *violent relaxation* because of the strong oscillations affecting the mean field [37]. The basic idea is that a given initial density distribution, which is not a stationary solution of the Vlasov equation, undergoes strong oscillations that bring it into a quasi-stationary state. Despite the underlying dynamics, such a state represents, to a certain extent, a macroscopic steady state, which would then explain the regularity of light emitted by elliptical galaxies. However, the quasi-stationary state exists only in a coarse-grained sense, i.e., at a finite resolution imposed by experiments or computer simulations, and does not allow to see the full fine-grained evolution of the distribution function. The coarse-grained version of the one-particle distribution function is thus expressed by

$$\bar{f}(\boldsymbol{q},\boldsymbol{p},t) = \frac{1}{(\Delta q \Delta p)^d} \int_{\Delta q \Delta p} f(\boldsymbol{q}',\boldsymbol{p}',t)\,\mathrm{d}\boldsymbol{q}'\,\mathrm{d}\boldsymbol{p}'\,, \tag{3.1}$$

where, $\Delta q \Delta p$ is the resolution of the coarse-grain.

The Lynden-Bell proposal is to find a configuration for $\bar{f}(\boldsymbol{q},\boldsymbol{p},t)$ that maximizes the coarse-grained version of entropy. Formally, this can be achieved by discretizing the initial density distribution function into different levels. The phase space is then divided into macrocells, which are in turn subdivided into microcells – each microcell containing up to one density level. All macroscopic observables are defined at the macrocell level, while the incompressibility intrinsic to Vlasov's dynamics prevents more than one-level from occupying a given microcell. This is shown schematically in Figure 4, where the phase space has been restricted to two dimensions.

For simplicity, consider a one-level distribution function whose density is η discretized on a two-dimensional grid whose microcells have area h^2. The volume fraction occupied by the level η inside the macrocell i is

$$\rho(q,p) = \frac{n_i}{\nu}, \tag{3.2}$$

where n_i is the number of microcells within the ith macrocell whose density level is η, such that $\rho(q,p)$ is less than or equal to one. The volume fraction is related to the distribution function by

$$\bar{f}(q,p) = \eta\,\rho(q,p). \tag{3.3}$$

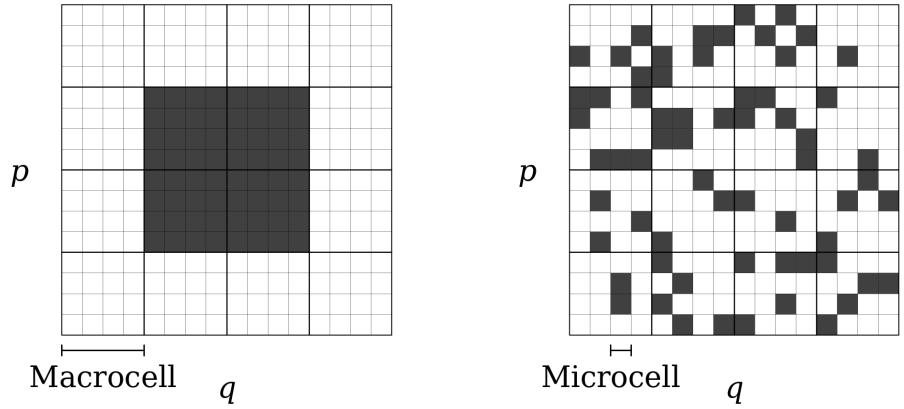

Figure 4 – Schematic representation of the phase space evolution of the density levels. The left panel shows the phase space representation of the initial state of an one-level distribution function, while the right panel shows the phase space at a later time. The total number of microcells occupied by each density level remains the same, but the macrocell density varies.

Consider now all possible configurations for which there are n_i density levels within the ith macrocell. The first of the n_i density levels can be distributed in ν ways, the second in $\nu - 1$ ways, and so on. Thus, the number of ways to assign the microcells to all n_i density levels is

$$\frac{\nu!}{(\nu - n_i)!} \tag{3.4}$$

The number of density levels in the phase space is always kept constant and equal to $N = \sum_i n_i$. Then the total number of microstates W corresponding to the macrostate in which n_i microcells are occupied in the ith macrocell is given by the product of all terms (3.4) with the number of ways of splitting the total number N into groups of n_i, i.e.,

$$W(\{n_i\}) = \frac{N!}{\prod_i n_i!} \times \prod_i \frac{\nu!}{(\nu - n_i)!} \tag{3.5}$$

Finally, the coarse-grained entropy of the system is defined as $\bar{s} \equiv -k_B \ln W$, where k_B is the Boltzmann constant. In the limiting case where the variations of $\bar{f}/\eta$ between macrocells are infinitesimal, i.e.,

$$\sum_i \to \int \frac{\mathrm{d}q\,\mathrm{d}p}{h^2}, \tag{3.6}$$

and using the Stirling approximation, the entropy can be written as

$$\bar{s} = -k_B \int \mathrm{d}q\,\mathrm{d}p \left[\frac{\bar{f}}{\eta} \ln\left(\frac{\bar{f}}{\eta}\right) + \left(1 - \frac{\bar{f}}{\eta}\right) \ln\left(1 - \frac{\bar{f}}{\eta}\right) \right], \tag{3.7}$$

apart from an additive constant. Here, the arguments of the coarse-grained distribution function $\bar{f}(q, p)$ are omitted for the sake of clarity.

Similar to the standard thermodynamic equilibrium, LB proposed that the steady state of a LR interacting system corresponds to the most likely distribution of density levels among macrocells. The assumption that microcells are free to move within different macrocells is consistent with the ergodicity hypothesis. In practice, however, it appears that dynamic effects may impede mixing [34, 33]. Nevertheless, the entropy given by (3.7) is a function of the coarse-grained distribution function, i.e., $\bar{s} \equiv s[\bar{f}]$, and can therefore be maximized, subject to the usual constraints of conservation of energy, mass (or number of particles), and other particular quantities such as the momentum of the system under study. Lynden-Bell's maximum entropy principle therefore leads to a constrained variational problem that can be solved with Lagrange multipliers.

3.1 Lynden-Bell's Maximum Entropy Principle for Continuous Distributions

With the theory discussed so far, the basic ideas have essentially been established, but specifically for a one-level distribution function. Moreover, the number of ways to assign N occupied microcells to all macrocells, the first term on (3.5), is calculated exactly as for Boltzmann gas [29], since the occupied microcells are distinguishable. On the other hand, the number of ways to assign n_i occupied microcells to the ith macrocell was calculated as a Fermi-Dirac-like statistic – seeing that the microcells cannot be occupied more than once. One might consider a Bose-Einstein-like statistic, for which the expression (3.4) would be ν^{n_i}. However, this is not the case here, since the interest is on the Vlasov dynamics, whose incompressibility property is well represented by the exclusion principle at the microcell level. It should be noted, however, that the method can be adapted to different statistics.

For continuous distributions, where the number of density levels can theoretically go to infinity, an expression is required which takes into account the many different levels. Consider n levels of phase density f_j, for $j \in \{1, \ldots, n\}$. The number of elements with density f_j located at the ith macrocell is then defined as n_{ij}. Clearly the total number of microcells occupied by the the level f_j is $N_j = \sum_i n_{ij}$ and the total number of occupied microcells is $N = \sum_j N_j$.

The number of ways to assign the microcells to all n_{ij} density levels within the ith macrocell is therefore

$$\frac{\nu}{(\nu - \sum_j n_{ij})!}. \tag{3.8}$$

Then, the number of microstates W compatible with the single macrostate defined by the numbers $\{n_{ij}\}$ is the product of all terms (3.8) with the number of ways of splitting the

pool of available N_j elements into groups of n_{ij}, which gives

$$W(\{n_{ij}\}) = \prod_j \frac{N_j!}{\prod_i (n_{ij})!} \times \prod_i \frac{\nu!}{(\nu - \sum_j n_{ij})!} \tag{3.9}$$

Finally, the entropy $s_{lb} = \ln \Omega$, which is rescaled by ν takes the form,

$$s_{lb} = -\sum_i \sum_j \frac{n_{ij}}{\nu} \ln \frac{n_{ij}}{\nu} - \sum_i \left(1 - \sum_j \frac{n_{ij}}{\nu}\right) \ln \left(1 - \sum_j \frac{n_{ij}}{\nu}\right), \tag{3.10}$$

apart from some constants.

3.2 A Monte Carlo Method to Solve Lynden-Bell's Maximum Entropy Principle

A numerical technique for maximizing Lynden-Bell entropy (3.10) is presented. It is based on the random exchange of density levels at the microcell level. For simplicity, the methods presented in this section are again restricted to two-dimensional phase spaces. However, they can be easily generalized to higher dimensions. In addition, an Euler fluid is considered in this section, but only the essential details of the system are presented here; it will be fully explored in the next chapter.

3.2.1 Elements of Fluid Dynamics

The equations for a two-dimensional incompressible fluid are the Navier-Stokes equation together with the incompressible condition. When there are no external forces and no viscosity, the Navier-Stokes equation becomes the so-called Euler equation. In the vorticity-stream formulation it is written as

$$\frac{\partial \Gamma}{\partial t} + (\boldsymbol{u} \cdot \boldsymbol{\nabla})\Gamma = 0, \tag{3.11}$$

$$\boldsymbol{\nabla} \cdot \boldsymbol{u} = 0, \tag{3.12}$$

where $\Gamma = (\boldsymbol{\nabla} \times \boldsymbol{u}) \cdot \hat{k}$ is the vortex density, $\boldsymbol{u}(\boldsymbol{r}, t)$ is the fluid velocity, $\hat{k}$ is the unit vector normal to the plane of the fluid, and the coordinate is thus $\boldsymbol{r} = x\hat{\imath} + y\hat{\jmath}$. The incompressible condition (3.12) allows the introduction of the stream function ψ, so that $\boldsymbol{u}(\boldsymbol{r}) = \boldsymbol{\nabla} \times \psi(\boldsymbol{r})\hat{k}$ yields the equations of motion

$$\dot{x} = +\,\partial\psi/\partial y\ , \tag{3.13}$$

$$\dot{y} = -\,\partial\psi/\partial x\ , \tag{3.14}$$

as well as Poisson's equation, if one applies the definition of the vortex density,

$$\nabla^2 \psi(\boldsymbol{r}, t) = -\Gamma(\boldsymbol{r}, t). \tag{3.15}$$

The solution of Poisson's equation can be easily found with the help of Green's function $G(\boldsymbol{r}, \boldsymbol{r}')$ of the Laplacian operator [2], which in open space (infinite domain) takes the form

$$G(\boldsymbol{r}, \boldsymbol{r}') = -\frac{1}{2\pi} \ln |\boldsymbol{r} - \boldsymbol{r}'| \,. \tag{3.16}$$

Therefore, the solution of (3.15) is

$$\psi(\boldsymbol{r}, t) = \int \mathrm{d}\boldsymbol{r}' \, \Gamma(\boldsymbol{r}', t) \, G(\boldsymbol{r}, \boldsymbol{r}'), \tag{3.17}$$

$$= -\frac{1}{2\pi} \int \mathrm{d}\boldsymbol{r}' \, \Gamma(\boldsymbol{r}', t) \ln |\boldsymbol{r} - \boldsymbol{r}'| \,. \tag{3.18}$$

Moreover, the energy is a conserved quantity of the Euler equation and is given by

$$H = \int \mathrm{d}\boldsymbol{r} \, \frac{1}{2} \left(\dot{x}^2 + \dot{y}^2 \right) \tag{3.19}$$

$$= \int \mathrm{d}\boldsymbol{r} \, \frac{1}{2} \left(\boldsymbol{\nabla} \psi \right)^2 \tag{3.20}$$

$$= -\frac{1}{2} \int \mathrm{d}\boldsymbol{r} \, \Gamma(\boldsymbol{r}) \, \psi(\boldsymbol{r}) \tag{3.21}$$

$$= -\frac{1}{4\pi} \iint \mathrm{d}\boldsymbol{r} \, \mathrm{d}\boldsymbol{r}' \, \Gamma(\boldsymbol{r}) \, \Gamma(\boldsymbol{r}') \ln |\boldsymbol{r} - \boldsymbol{r}'| \,. \tag{3.22}$$

Here the solution of Poisson's equation was introduced instead of $\psi(\boldsymbol{r})$.

This expression for the energy highlights the pairwise logarithmic interaction, which corresponds to a power law decay with an effective exponent $\delta = 0$; characterizing the system as one with LR interactions, since the dimension of the embedded space $d = 2$ is greater than δ.

Further conserved quantities are the total vorticity and the angular momentum. Respectively,

$$\Gamma_t = \int \mathrm{d}\boldsymbol{r} \, \Gamma(\boldsymbol{r}), \tag{3.23}$$

$$L = \int \mathrm{d}\boldsymbol{r} \, \Gamma(\boldsymbol{r}) \|\boldsymbol{r}\|^2, \text{ and} \tag{3.24}$$

3.2.2 The Stochastic Entropy Maximization Algorithm

For the initial one-level waterbag distribution of vortices, the Lynden-Bell distribution corresponding to the state of maximum entropy can be explicitly calculated under the constraints of the given conserved quantities,

$$f_{lb}(\boldsymbol{r}) = \frac{\eta}{1 + \exp\Big\{\eta(\beta\psi(\boldsymbol{r}) + \alpha\|\boldsymbol{r}\|^2 - \mu))\Big\}}, \tag{3.25}$$

where η is the density of the waterbag distribution, $\psi(\boldsymbol{r})$ is the stream function associated to the distribution through the Poisson equation (3.15), and β and α are the Lagrange multipliers which are connected with the energy and the angular momentum, respectively.

Solving the Poisson equation using (3.25) as the source function and taking into account the conserved quantities yields the Lagrange multipliers as well as the distribution function itself.

The Lynden-Bell statistical approach allows the explicit calculation of solutions of the Vlasov equation, taking into account constraints such as those shown here. However, for an arbitrary initial flow, this would require an infinite number of Lagrange multipliers, which makes the solution of the Linden-Bell equations very difficult. For this reason, an algorithm was developed to determine the Lynden-Bell equilibrium in a simple way using a Monte Carlo approach (MC).

The algorithm, called Stochastic Entropy Maximization Algorithm (SEMA), is based on the canonical MC method with two Lagrange multipliers α and β – the first to preserve the total angular momentum and the second to preserve the total energy in the system. To find the equilibrium distribution in the framework of LB's theory, the initial vorticity distribution, in this case $f(x, y)$, is discretized into the coarse-grained function $\bar{f}(i, j)$ whose domain is a regular M×N grid. This rectangular lattice is formed from the tensor product of two uniform regular grids of (L, L):

$$\{x_i = (i - 0.5)h_x - L, \quad i = 1, \ldots, M, \quad h_x = 2L/M\}, \tag{3.26}$$

$$\{y_j = (j - 0.5)h_y - L, \quad j = 1, \ldots, N, \quad h_y = 2L/N\}. \tag{3.27}$$

such that the coordinate (x, y) in the phase space maps to the center node of the ij-cell in the Eulerian mesh, that is, $f(x, y) \to \bar{f}(i, j)$, or $\bar{f}_{ij}$ for short. Each of the lattice's cells contains ν microcells, for which the density of the microcell of index k is η_k, and the density at coordinate (i, j) is simply the arithmetic mean over all its microcells

$$\bar{f}_{ij} = \frac{1}{\nu} \sum_{k=1}^{\nu} \eta_{ij,k} \tag{3.28}$$

At the beginning, the density levels are set to a value identical to the distribution function in the corresponding coordinate, i.e., $\eta_{ij,k} = f(x_i, y_j)\ \forall\ k \in \{1, \ldots, \nu\}$, so that all the microcells within a macrocell (i, j) have exactly the same density level. The stream function ψ_{ij} produced by the density distribution function $\bar{f}_{ij}$ is computed on an identical M×N Eulerian mesh at the macrocell level using the discrete Poisson equation,

$$\begin{aligned} (\Delta\psi)_{ij} &= -2\pi \bar{f}_{ij}, \\ (D^2_{xx}\psi)_{ij} + (D^2_{yy}\psi)_{ij} &= -2\pi \frac{1}{\nu} \sum_{k=1}^{\nu} \eta_{ij,k}, \end{aligned} \tag{3.29}$$

where the second central difference operator is denoted by

$$(D^2_{xx}\psi)_{ij} \equiv \frac{\psi_{i+1,j} - 2\psi_{i,j} + \psi_{i-1,j}}{h_x^2}, \text{ and} \tag{3.30}$$

$$(D^2_{yy}\psi)_{ij} \equiv \frac{\psi_{i,j+1} - 2\psi_{i,j} + \psi_{i,j-1}}{h_y^2}, \tag{3.31}$$

with Dirichlet boundary conditions within a disk D of radius L, $\partial D = 0$. The total energy and angular momentum of the initial distribution are respectively:

$$E_0 = h_x h_y \frac{1}{2} \sum_{i,j} \bar{f}_{ij} \psi_{ij} \tag{3.32}$$

$$L_0 = h_x h_y \sum_{i,j} \bar{f}_{ij} r_{ij}^2 \tag{3.33}$$

The basic steps of SEMA are as follows:

1. Select two macrocells at random. The first macrocell is selected and then removed from a list containing all macrocells of the grid; then

2. For each of the selected macrocells, select a microcell at random. If a microcell is empty its density level is zero. If the chosen density levels are the same, go back to the first step; otherwise

3. Compute the energy and angular momentum variation for the attempted exchange:

$$\delta E = (\eta_{\mathrm{A},1} - \eta_{\mathrm{B},2}) \times (\psi_{\mathrm{A}} - \psi_{\mathrm{B}}), \tag{3.34}$$

$$\delta L = (\eta_{\mathrm{A},1} - \eta_{\mathrm{B},2}) \times \left(r_{\mathrm{A}}^2 - r_{\mathrm{B}}^2\right), \tag{3.35}$$

   where A and B refer to the macrocells containing microcells 1 and 2, respectively. r^2 is the square distance from the origin to the center of the macrocell and ψ is the stream function; next

4. Evaluate the acceptance condition. The Metropolis algorithm establishes the acceptance criterion for the exchange,

$$\mathrm{e}^{-\beta\delta E - \alpha\delta L} > P(X), \tag{3.36}$$

   where P(X) is a uniform random number between 0 and 1. Starting with an initial guess, the Lagrange multipliers β and α must be adjusted so that the energy and angular momentum are conserved.

5. Perform steps 1. through 4. until all coordinates are chosen exactly one time. This defines a Monte Carlo step (MCS) – a cycle in which at least one microcell in each coordinate of the grid is tested against the acceptance condition and given a chance to exchange density with another randomly selected microcell. Then, reinitialize the list used in the first step;

6. After each MCS the values of $\bar{f}$ and ψ are updated. The Lagrange multipliers are updated as:

$$\beta^{(new)} = \beta^{(old)} + \sigma_E (E - E_0)/E_0, \tag{3.37}$$

$$\alpha^{(new)} = \alpha^{(old)} + \sigma_L (L - L_0)/L_0. \tag{3.38}$$

Where E and L are respectively the energy and angular momentum of the current iteration; and E_0 and L_0 are the conserved values of these quantities. The parameter σ controls the speed of updates. The updates will stop when both energy and angular momentum converge to the target values E_0 and L_0.

The choice of an appropriate exchange mechanism, i.e., the set of acceptance conditions plus constraints (steps 4. and 6.) is imperative. For example, the choice of Lagrange multipliers leads to constraints on the energy and angular momentum in step 6. Note that the signals in equations (3.37) and (3.38) have meaning. When the values of energy or angular momentum are larger than in the initial constraint, the increase in β or α expresses the intention to accept positive exchanges for these quantities with a lower probability.

For an one-level waterbag vorticity, the initial condition and the equilibrium density distribution obtained using SEMA is plotted in Figure 5, where the radial density distribution is also plotted. As seen, the results of SEMA are in excellent agreement with the numerical solution of LB theory.

The advantage of SEMA is that it automatically takes into account different density levels of the initial distribution, whereas in a direct entropy maximization these have to be considered as an infinite set of Lagrange multipliers. For example, in Figure 6 relaxation of the initial distribution $f(x, y) \propto \exp(-x^4 - 16y^4)$ is studied. The equilibrium density distribution calculated using SEMA is show in Figure 6b, while the radial density distribution function is shown in Figure 6c.

The results presented in this section were obtained using a square grid with dimensions M, N equal to 512, number of microcells per macrocell $\nu = 32$, and length of each macrocell $h_x = h_y = 0.0039L$. The stream function is calculated using the successive over-relaxation (SOR) iterative method [51]; more details are given in the next chapter.

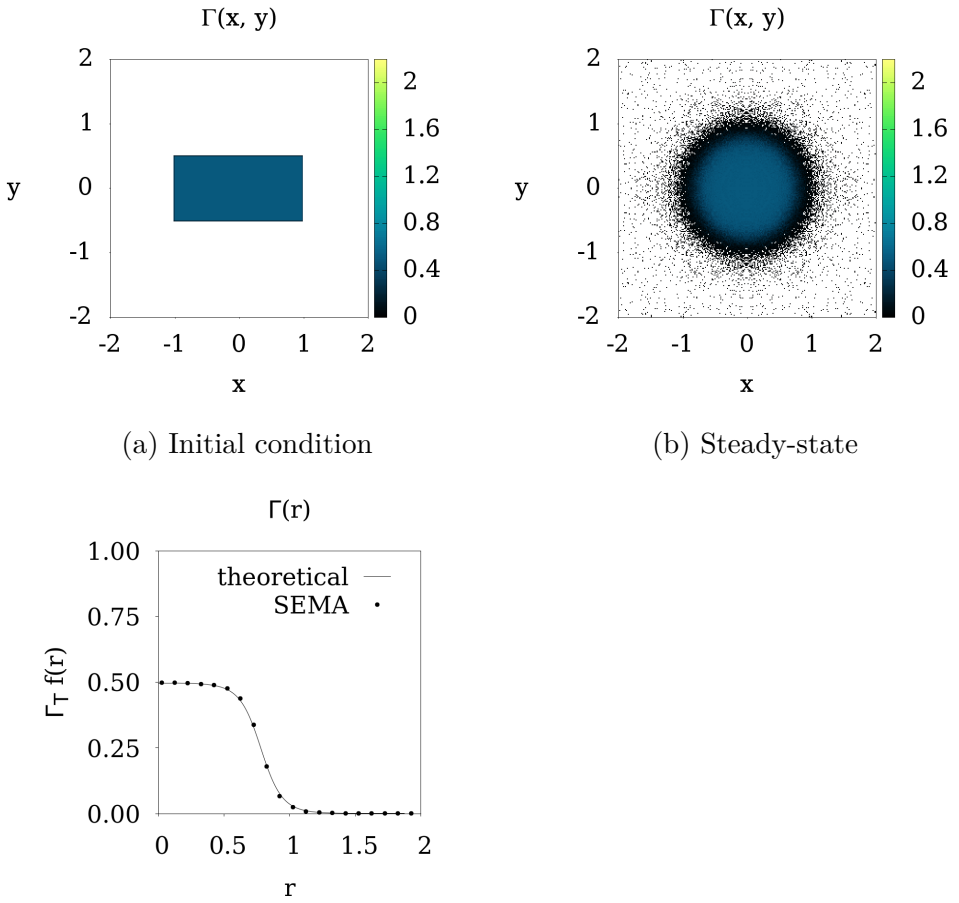

(a) Initial condition

(b) Steady-state

(c) Radial distribution

Figure 5 – Snapshots of the phase space obtained using SEMA. The initial condition is a one-level rectangular distribution function, $f(x, y) = 0.5\,\Theta\,(1.0 - |x|)\;\Theta\,(0.5 - |y|)$, normalized to unity. The steady-state is LB equilibrium, with radial distribution function shown in (c), obtained from the maximization of equation (3.25).

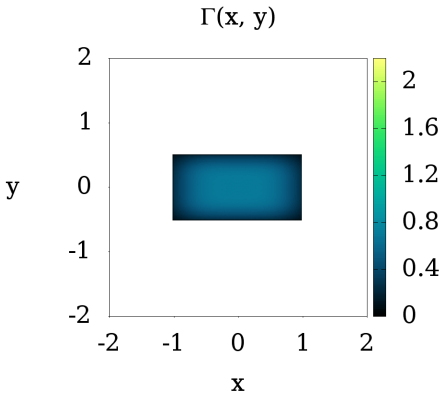

(a) Initial condition

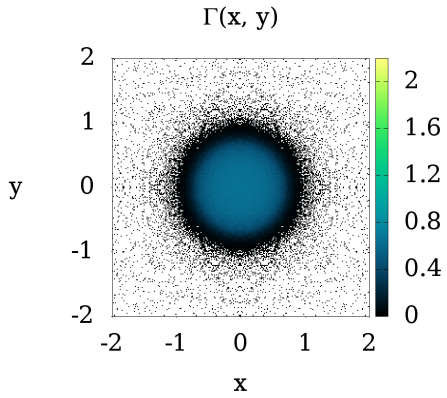

(b) Steady-state

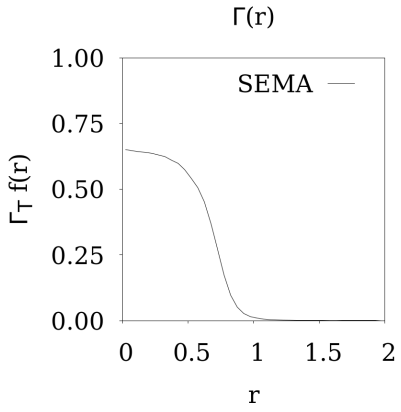

(c) Radial distribution

Figure 6 – Snapshots of the phase space obtained using SEMA. The initial condition is a continuous rectangular distribution function, $f(x, y) = 0.7\mathrm{e}^{-x^4-16y^4}\,\Theta\,(1.0 - |x|)\,\Theta\,(0.5 - |y|)$, normalized to unity. The steady state corresponds to LB equilibrium.

4 Two-dimensional Fluid Mechanics

Hydrodynamics is another important field where long-range interactions play a major role. This chapter deals specifically with two-dimensional high Reynolds number flows. At high Reynolds numbers, laminar flow becomes turbulent and spontaneous organization into coherent structures is observed. It should be noted, however, that three-dimensional flows, such as geophysical flows, also fall into the realm of long-range interactions but are fundamentally different: in three-dimensional flows, an energy cascade occurs where energy is dissipated as it moves from large to small scales, whereas in two-dimensional flows, the introduction of additional constraints, such as finite confined space, leads to an *inverse* energy cascade that results in a very small number of large structures.

Turbulent flows exhibit vortices, which are a special form of fluid motion represented as rotation of fluid elements – vorticity is therefore usually expressed as the rotational of the fluid velocity, although the mathematical formalism for defining vortices is controversial [55]. Vortices are ubiquitous in nature and can be observed in a wide variety of phenomena and in a large range of sizes. Examples include, from small to large sizes, super-fluid vortices, swirling flows in turbines, ocean eddies, tornadoes, Jupiter's Red Spot, and even spiral galaxies. Next, we examine Onsager's statistical approach to two-dimensional confined vortices, molecular dynamics simulations, and finally the description and application of an algorithm – similar to Lynden-Bell's entropy maximization algorithm developed in the previous chapter – to find steady states of two-dimensional Euler fluids.

4.1 Onsager's Point-Like Vortex Formalism

In his 1949 paper [46], Onsager argues for the possibility of equilibrium states with negative temperature. His theory is based on the approximation of the continuous Euler system by a large but finite number of point-like vortices – i.e. on the definition of vortex density as introduced by Helmholtz [28],

$$\Gamma(\boldsymbol{r}, t) = \sum_i \Gamma_i \, \delta \left[\boldsymbol{r} - \boldsymbol{r}_i(t) \right] . \tag{4.1}$$

And since the velocity of the point-like vortices must be equal to the velocity of the fluid at the same location, it follows that $\mathrm{d}\boldsymbol{r}/\mathrm{d}t = \boldsymbol{\nabla}_i \times \sum_{j \neq i} \Gamma_j \, G(\boldsymbol{r}_i, \boldsymbol{r}_j) \hat{k}$, where $G(\boldsymbol{r}_i, \boldsymbol{r}_j)$ is the Green's function solution to the Poisson equation (3.16), which also leads to a

Hamiltonian structure of the equations of motion,

$$\Gamma_i \frac{\mathrm{d}x_i}{\mathrm{d}t} = +\frac{\partial H}{\partial y_i}, \tag{4.2}$$

$$\Gamma_i \frac{\mathrm{d}y_i}{\mathrm{d}t} = -\frac{\partial H}{\partial x_i}, \tag{4.3}$$

defining the Kirchhoff function as

$$H = -\frac{1}{4\pi} \sum_i \sum_{j \neq i} \Gamma_i \Gamma_j \ln |\boldsymbol{r}_i - \boldsymbol{r}_j| \,. \tag{4.4}$$

The vortex fluid moves thus as an N-body system, where the trajectories of each vortex is usually very complicated. Nonetheless, the formation of large coherent structures suggests the possibility of an explanation on statistical grounds.

Onsager's logic is as follows: N vortices confined to a finite region A have a finite phase space volume A^N, and therefore the number of accessible microstates for a given energy E must be a non-monotonic function such that $\Omega(E)$ tends toward zero for both small and large E. This implies that there is a critical energy E_c for which $\Omega(E_c)$ is maximal. The critical energy corresponds to the most disordered arrangement of vortices, where they uniformly occupy the entire available area. In the framework of Boltzmann-Gibbs statistical mechanics, the microcanonical entropy is $S(E) = k_B \ln \Omega(E)$, which means that the inhomogeneous vortex distribution has a lower entropy for $E > E_c$ than at E_c. Since the absolute temperature is $1/T = \partial S(E)/\partial E$, decreasing entropy leads to a state with negative absolute temperatures. In conclusion, the presence of states with negative temperature implies the accumulation of vortices with the same sign of vorticity, which would explain the formation of large vortex structures in turbulent incompressible two-dimensional flows.

4.1.1 Issues with Osager's Statistical Approach

A fundamental theorem of fluid dynamics [39, 22] states that any smooth solution of two-dimensional Euler equation can be approximated over a finite time interval using N point-like vortices of vanishing vorticity $\Gamma_i \sim \pm 1/N$ in the limit $N \to \infty$. This corresponds exactly to the thermodynamic limit for systems with long-range interactions [15, 13, 35], and it is well known that such systems do not relax to thermodynamic equilibrium in the limit $N \to \infty$, which precludes the application of Boltzmann-Gibbs statistical mechanics. Therefore, Onsager's attempt to explain the formation of large structures in two-dimensional Euler fluids using standard arguments from statistical mechanics is invalid.

In the remainder of this chapter we will confine ourselves to flows with a circulation of only one sign. However, the theoretical considerations presented here can easily be extended to all flows containing both clockwise and counterclockwise vortices. Note that

if all vortices have the same vorticity $\Gamma_i = \Gamma_T/N$, where Γ_T is the total vorticity, the vortex equations of motion (4.2) and (4.3) can be further simplified to read respectively as (3.13) and (3.14). Then, consider $f(\boldsymbol{r}, t)$ the vortex distribution function. The vortex density can be written as $\Gamma(\boldsymbol{r}, t) \equiv \Gamma_T f(\boldsymbol{r}, t)$ if the distribution function is normalized to unity. Then, since the vortices are simply advected by the flow, as per (3.11), the distribution function satisfies the Vlasov equation,

$$\frac{\partial f}{\partial t} + \frac{\partial \psi}{\partial y}\frac{\partial f}{\partial x} - \frac{\partial \psi}{\partial x}\frac{\partial f}{\partial y} = 0. \tag{4.5}$$

Vlasov's dynamics will lead the system to a qSS, and any local functional $g[f]$ is conserved along the evolution,

$$C_f = \int g(f(\boldsymbol{r}, t))\, \mathrm{d}\boldsymbol{r}\,. \tag{4.6}$$

These are called Casimir invariants. In particular, the volume occupied by the different levels of the distribution function is a Casimir invariant of the Vlasov equation, suggesting that one could apply Lynden-Bell's theory of collisionless relaxation to the Euler hydrodynamics of a two-dimensional inviscid fluid. This idea will be explored in the Sect. 4.3 in the context of the core-halo model.

4.2 Molecular Dynamics Simulations

Simulations of two-dimensional vortex fluids were performed using molecular dynamics simulations (MD). The collisional nature of MD is a fundamental requirement for the hypothesis of residual correlation between particles. However, from the point of view of fluid dynamics, where only point-like vortices of infinitesimal strength are physically relevant, this is anything but ideal. Since the number N of particles in computer simulations is always finite, there are residual correlations between particles due to the force computation, especially when one considers a Hamiltonian (4.4), yielding equations of motion such as

$$\boldsymbol{u}_i = \frac{1}{2\pi}\sum_{j\neq i}^{N} \frac{(\boldsymbol{r}_i - \boldsymbol{r}_j) \times \Gamma_j\, \hat{k}}{r_{ij}^2}. \tag{4.7}$$

The finite pairwise vorticity leads to residual interactions, namely collisions, which can lead to unreliable results in the large time limit. Another major limitation of direct numerical integration of these equations of motion is the $O(N^2)$ order of the algorithm, which arises from the long-range interaction between vortices – since one cannot introduce a cutoff limit size or implement fast methods such as neighborhood searches and cell lists.

A hybrid MD simulation using an adaptive time-step integrator [1] and the particle-in-cell method [17, 20, 21], which allows the calculation of forces with a "smoothed" solution of the Poisson equation on a grid, is the alternative method used in this work. The basic

steps of the algorithm are the following: 1) the space is divided into an M×N rectangular grid and the vortex strength is assigned to each node located in the center of each grid cell; 2) the Poisson equation is solved on the lattice consisting of the nodes using an iterative method; 3) the force on each vortex is obtained by interpolating the potential obtained in the previous step; 4) a 5th order Runge-Kutta algorithm is used to advance the system by a time interval dt; 5) repeat until a steady-state is reached.

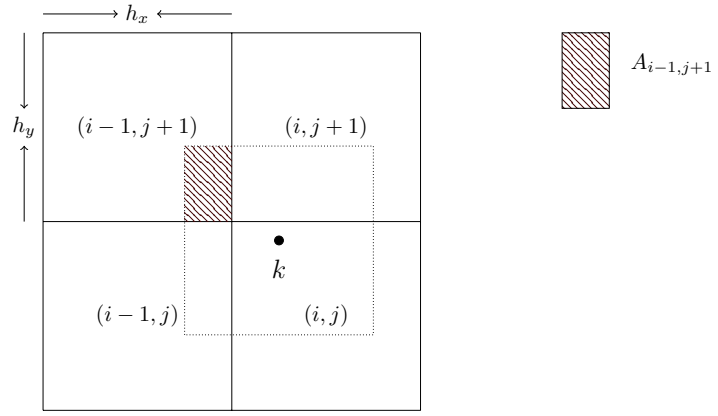

Figure 7 – Illustration of the grid representing the particle distribution in the first step of the particle-in-cell algorithm. The kth vortex, indicated by a black dot, shares its vorticity between the cell in which it is located and the neighboring cells that are within range of the PIC core. In the figure, the cell $(i-1, j+1)$ has a contribution proportional to the area $A_{i-1,j+1}$.

The first step is to construct a rectangular density lattice with regular nodes at the center of each cell. Each node is then assigned a vorticity according to the particle-in-cell algorithm. Next, the discrete Poisson equation is solved using an iterative technique based on the Gauss-Seidel method called successive over-relaxation (SOR) – both methods are used to solve a linear system of equations of the form $A\boldsymbol{x} = \boldsymbol{b}$, but the SOR includes a relaxation factor to speed convergence [27]. Decomposing the matrix A into a diagonal component D, plus the upper and lower triangular components, respectively U and L, results in $(D + U + L)\,\boldsymbol{x} = \boldsymbol{b}$. After a little algebra, it is then written as

$$(D + \omega L)\,\boldsymbol{x} = \omega\boldsymbol{b} - [\omega U + (\omega - 1)D]\;\boldsymbol{x}, \tag{4.8}$$

where ω is the relaxation factor constant, which must be greater than or equal to one and less than two. $\omega = 1$ recovers the Gauss-Seidel method. The triangular form, $(D+\omega L)$, on the left-hand side of the previous equation allows $\boldsymbol{x}$ to be solved iteratively, by computing the values $\boldsymbol{x}^{(n)}$ one at a time by forward substitution, as in the following equation,

$$\boldsymbol{x}^{(n+1)} = \frac{1}{D + \omega L}\Big\{\omega\boldsymbol{b} - [\omega U + (\omega - 1)D]\,\boldsymbol{x}^{(n)}\Big\}. \tag{4.9}$$

The discrete Poisson equation is then solved numerically by the above equation, where $\boldsymbol{x}$ represents the unknown potential at the potential lattice nodes and $\boldsymbol{b}$ represents the density lattice. The matrix $A \equiv D + U + L$ describes the finite difference approximation of the Laplacian in the Poisson equation according to a two-dimensional five-point stencil, which means that the potential must be smooth only when considering the first neighbors. Rewriting (4.9) for each component $x_i^{(n)}$ yields

$$x_i^{(n+1)} = (1-\omega)x_i^{(n)} + \frac{\omega}{a_{ii}}\left(b_i - \sum_{j<i} a_{ij}x_j^{(n+1)} - \sum_{j>i} a_{ij}x_j^{(n)}\right), \tag{4.10}$$

where a_{ij} are the components of the matrix A, and b_i are the components of the vector $\boldsymbol{b}$. The estimate of the error of the method is of the order of $O(h^2)$, where $h^2 \equiv h_x h_y$ is the area of the cell. The complete description of the SOR algorithm is found at Ref. [6]. By interpolating the potential, the force acting on each vortex is calculated and the position of the vortices is updated by the fifth-order Runge-Kutta algorithm [1]. All MD simulations in this thesis were performed with a number $2^{23} \equiv 8388608$ of point-like vortices, a 512×512 gridsize, and Dirichlet boundary conditions within a disk D of radius L, $\partial D = 0$. The length of each cell is $h_x = h_y = 0.0039L$.

4.3 The Core-Halo Statistical Approach

The core-halo theory was introduced to explain the relaxation of an elliptical Kirchhoff vortex in a rotating reference frame. Recall that Kirchhoff vortices rotate like a rigid body with a constant angular velocity. In addition, a highly eccentric elliptical vortex patch is susceptible to linear instabilities [36, 11], but even low eccentricity elliptical Kirchhoff vortices are susceptible to non-linear instabilities in which the vortices close to the border enter in resonance with the rotation of the Kirchhoff vortex and are ejected from the vortex [47], see Figure 8.

Since the Kirchhoff function (4.4) depends only on x and y coordinates, the vortices that are ejected end up with lower energy than vortices that are inside the core region. The process of evaporative heating results in the reorganization of the core region and formation of a core-halo structure. The situation becomes clearer if we transform into the reference frame that rotates together with the vortex patch: $(x, y) \to (\tilde{x}, \tilde{y})$,

$$\tilde{x} = +x\cos(\omega t) + y\sin(\omega t), \tag{4.11}$$

$$\tilde{y} = -x\sin(\omega t) + y\cos(\omega t). \tag{4.12}$$

with ω the angular velocity with which an elliptical Kirchhoff vortex rotates. The canonical coordinate transformation can be described by the generating function,

$$\mathcal{F}(x, \tilde{y}) = \frac{x\tilde{y}}{\cos(\omega t)} + \frac{x^2 + \tilde{y}^2}{2}\tan(\omega t), \tag{4.13}$$

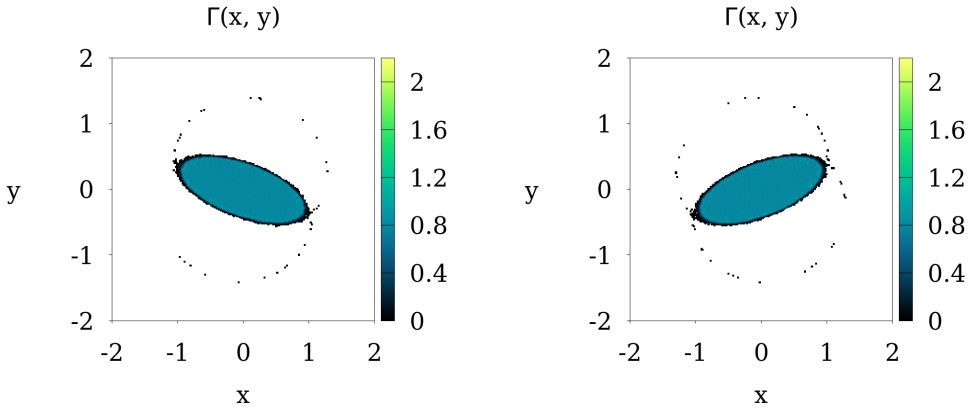

Figure 8 – Snapshots of the phase space obtained using MD simulation. The figures show the early stages of evolution of the initial condition $f(x,y) = (2.5/\pi)\,\Theta\,(1.0 - x^2 - 6.25y^2)$. Notice that even without linear instabilities, vortices are ejected and concentrate in the resonant region.

such that $\tilde{x} = \partial\mathcal{F}/\partial\tilde{y}$ and $y = \partial\mathcal{F}/\partial x$. Since the generating function has an explicit time dependence, the stream function in the rotating reference frame will be

$$\widetilde{\psi}(\tilde{x},\tilde{y}) = \psi(\tilde{x},\tilde{y}) + \frac{\omega}{2}\left(\tilde{x}^2 + \tilde{y}^2\right). \tag{4.14}$$

Figure 9 shows the equipotential curves corresponding to the stream function in the laboratory frame and in the rotating reference frame. It can be seen that the surface of the ellipse does not represent an equipotential in the laboratory frame, while it becomes an equipotential in the rotating reference frame for a certain value of ω. This means that it is possible to write the distribution function so that the dependence on the coordinates appears only by $\widetilde{\psi}(x,y)$. This means that the rotating elliptic Kirchhoff vortex is a stationary solution – in the rotating reference frame – of the Vlasov equation. In the thermodynamic limit, the Kirchhoff vortex would rotate forever. In practice, however, it is susceptible to small perturbations that can lead to linear and non-linear instabilities [11, 54, 41, 23]. The perturbed vortices are caught by the isopotential path of the separatrix, leading to vortex evaporation and halo formation, see Figure 9b.

The separatrix orbit traps vortices that are near the elliptical edge and moves them into low-energy regions of phase space, where they form a halo, while other vortices compensate by moving into high-energy regions within the core. This leads to a population inversion in the core region. This process continues until all the high energy levels inside the core up to the Fermi energy are completely occupied and a completely degenerate cold core is formed. In the present case, we consider the cold to be $T \to 0^-$, which is consistent with Onsager's idea of negative temperature. The final state is a characteristic core-halo structure with a population-inverted core region. Observations from MD simulations show that the core is not always completely frozen and the system is dynamically trapped.

In the laboratory frame, halo formation follows a filamentation process, as can be seen from the simulation of MD – see Figure 10. When the original vortex patch relaxes,

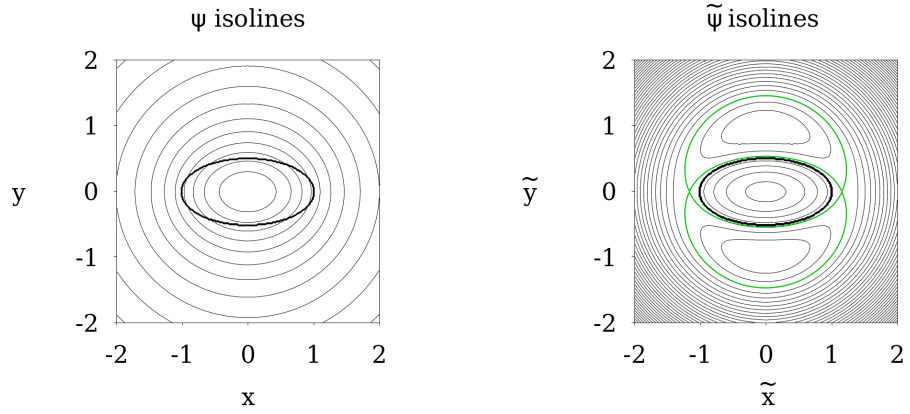

(a) Laboratory ref. frame (b) Rotating ref. frame

Figure 9 – Isolines of the potentials (thin lines) produced by a Kirchhoff's vortex (thick lines). The transformed potential exhibit a separatrix between high- and low-potential regions (green lines on the right panel).

the vortices are captured by resonance and follow the separatrix path that leads them away from the core region. Evaporation disturbs the rotation of the core, affecting the resonance orbit (separatrix), which moves inward. While the ejected vortices migrate to the low-energy region of phase space, the vortices in the core rearrange themselves so that the total energy is conserved. However, due to the incompressibility constraint imposed by the Vlasov dynamics, the process cannot continue indefinitely, and at some point the core will be frozen – all of the free energy released by the evaporated vortices will result in a completely degenerate core in which all of the highest energy states up to the Fermi energy are occupied. At this point, the process of evaporative heating must come to an end. In practice, one often sees incomplete relaxation where the core does not reach a fully degenerate frozen state.

To solve the core-halo model, the stream function produced by the particle distribution with a core-halo structure must be computed self-consistently. The core temperature is $T \to 0^-$, which requires that the occupation of energy levels within the stream function follows a hierarchical structure in which the higher density levels are closer to the core center than the lower density levels. At the same time, a process of vortex evaporation takes place, leading to the formation of a halo. In principle, it is possible to write down the equations that allow a self-consistent calculation of the core-halo structure, taking into account the conservation of total energy and total momentum, as well as the volume occupied by all density levels of the initial distribution function. In practice, however, it is easier to solve the core-halo theory with a stochastic algorithm, similar to what was done in Chapter 3 for the LB theory. Here, the algorithm is referred to as the Stochastic Core-Halo Algorithm (SCHA). The algorithm is based on the following subdivision of the phase space: in the rotating reference frame, the configuration space is divided into two active regions, namely core and halo, in which density levels are allowed to remain.

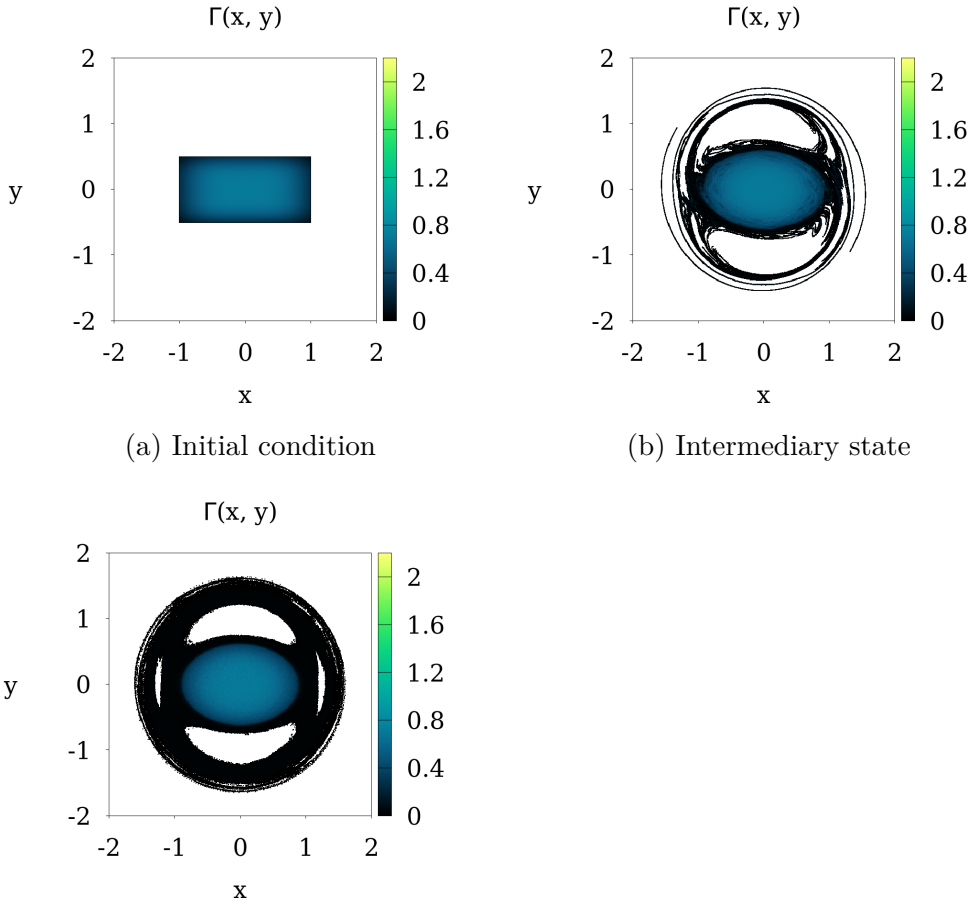

(a) Initial condition

(b) Intermediary state

(c) Steady-state

Figure 10 – Snapshots of the phase space obtained using MD simulation. The initial condition is a continuous rectangular distribution function, $f(x,y) = 0.7\mathrm{e}^{-x^4-16y^4}\,\Theta\left(1.0-|x|\right)\,\Theta\left(0.5-|y|\right)$, normalized to unity. The final state is a steady-state whose core regions accounts for about 92.5% of the total density

The separatrix then divides the configuration space into a high-energy inner region and a low-energy outer region. The core corresponds to an inner, maximally packed, cold region bounded by a Fermi energy ε_F, and the halo corresponds to a low density non-uniform region extending from the inner region to the outer region where it is bounded by the halo energy ε_H – the halo energy is defined as the value of the isopotential of the separatrix corresponding to the initial distribution. The angular velocity of the vortex patch (rotating reference frame) is calculated using the inertia tensor of the distribution:

$$\mathbf{I} = \begin{bmatrix} \langle x^2\rangle & -\langle xy\rangle \\ -\langle xy\rangle & \langle y^2\rangle \end{bmatrix} \tag{4.15}$$

The angle θ between the x-axis and the major principal axis of the distribution can be found using the arctan function and the components of one of the eigenvectors computed

from the inertia matrix (4.15),

$$\theta = \arctan\left(\frac{2\langle xy\rangle}{\langle y^2\rangle - \langle x^2\rangle - \sqrt{4\langle xy\rangle^2 + (\langle x^2\rangle - \langle y^2\rangle)^2}}\right), \tag{4.16}$$

The instantaneous angular velocity can be calculated as the time derivative of θ. Assuming that the distribution is axisymmetric and that the principal axis coincides with x and y axes at the time of measurement, so that $\langle xy\rangle \to 0$, yields

$$\omega = \frac{\mathrm{d}\theta}{\mathrm{d}t} = -\frac{\langle \dot{xy}\rangle}{\langle x^2\rangle - \langle y^2\rangle} = -\frac{\langle x\dot{y} + y\dot{x}\rangle}{\langle x^2\rangle - \langle y^2\rangle}. \tag{4.17}$$

The Eulerian mesh/discretized version of the above equation can be written as:

$$\omega \equiv -\frac{\sum_{i=1}^{M}\sum_{j=1}^{N}\bar{f}_{ij}\left(x_i\dot{y}_j + y_j\dot{x}_i\right)}{\sum_{i=1}^{M}\sum_{j=1}^{N}\bar{f}_{ij}\left(x_i^2 - y_j^2\right)} \tag{4.18}$$

where M and N are the dimensions of the Eulerian mesh.

Unlike the elliptical Kirchhoff vortex patch, the steady-state angular velocity of an arbitrary initial distribution is not known a priori. For example, the isopotential lines shown in Figures 11a and 11b are only approximations, since the rectangular vortex patch undergoes distortion in the early stages of evolution and does not rotate as a rigid body. The isopotentials were calculated using (4.14) with angular velocity ω from the actual particle distribution functions obtained from MD simulation using (4.18). It can be seen that the point-like vortices in the MD simulation clearly follow the trajectories described by the isopotential lines. Figure 11c shows that even when the dynamics in the core region have long stopped, the halo continues to evolve through the process of filamentation. Since the halo is so tenuous and has a *quasi*-circular symmetry, it does not contribute significantly to the resulting angular velocity.

From the structure of the isopotentials, we see that the core exists only in the inner region, while the halo extends between the inner and outer regions. This is shown in Figure 12. The core is defined as the inner region whose potential is above the Fermi energy ε_F, which will be calculated self-consistently as will be described below. The halo region is defined as the inner region whose potential is below ε_F plus the outer region whose potential is between the halo energy ε_h and the separatrix region ε_s, see Figure 12b. Core and halo belong to the *active* regions, namely the regions for which density level exchanges is allowed. Density levels may also be found in the inactive regions – outside the core and halo – due to initial distribution or due to previously active regions becoming inactive as the separatrix moves inward. Therefore, transfer from inactive to active regions is allowed, but not vice versa.

The rules of SCHA are very simple. An exchange between density levels involving a microcell within the core region is allowed only if it increases the total energy. Note that the energy change is calculated in the rotating reference frame. In addition, with

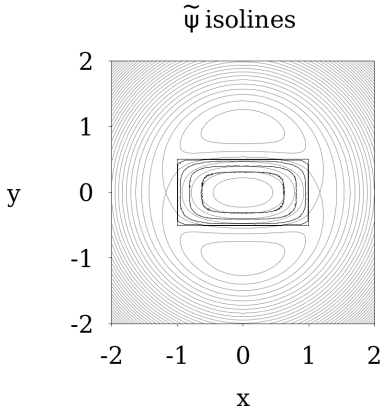

(a) Initial condition

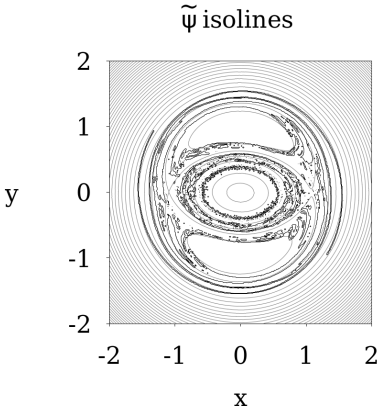

(b) Intermediary state

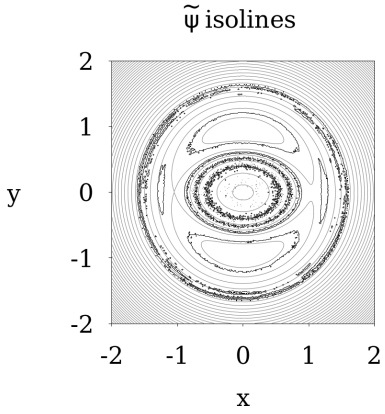

(c) Steady-state

Figure 11 – Contour plots, in the rotating reference frame with ω calculated using equation (4.18), of the stream function (thin lines) and of isodensities (points) obtained using MD simulation and equation (4.14). The panels correspond to the contour plots in Figure 10. The final steady-state exhibits exact isopotentials, while in the initial and intermediary states isopotential curves are approximate, since the distribution functions undergoes distortion as it rotates. One can see that vortices rearrange themselves by spreading along the equipotential lines.

the exception of the first move, all exchanges must compensate for the change in angular momentum, i.e., if the previous move resulted in an excess of angular momentum, only exchanges that decrease the total angular momentum are accepted, and vice versa. In this way, the angular momentum should be preserved during SCHA. Random exchange of levels within halo macrocells is allowed. After one MCS the stream function and angular velocity are recalculated. Finally, the Fermi energy is updated

$$\varepsilon_F^{(new)} = \varepsilon_F^{(old)} + \sigma_E(E - E_0)/E_0\,, \tag{4.19}$$

where E is the current iteration energy and E_0 is the energy of the initial distribution that must be conserved. In the present work we used $\sigma_E = 1$ for the speed of updates. In SCHA the Fermi energy acts as a Lagrange multiplier which is adjusted so that the

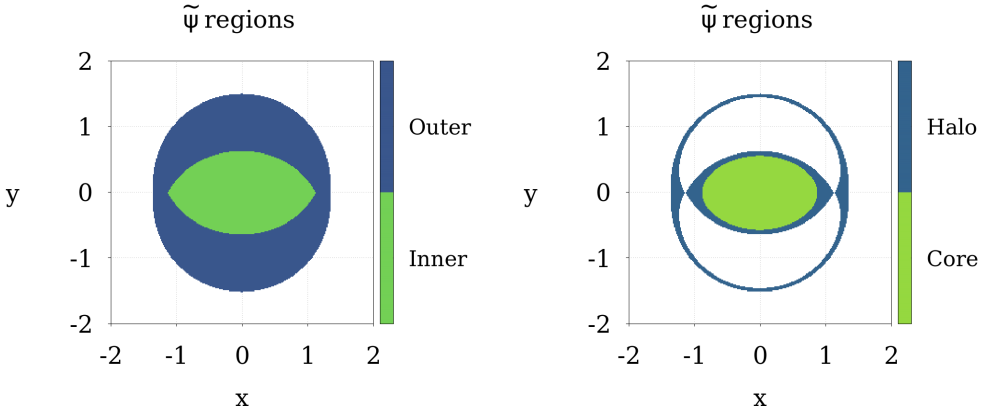

(a) inner and outer regions

(b) core and halo regions

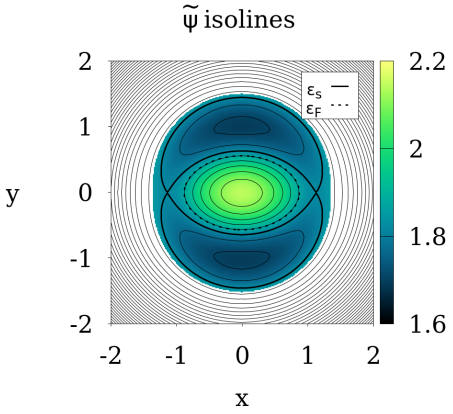

(c) isopotentials of $\widetilde{\psi}$

Figure 12 – Contour plot of the stream function and divisions of phase space into abstract regions: (a) shows the division of the phase space into inner and outer regions. The interface between them is defined by the separatrix, while the outer region is also bounded externally by ε_h; (b) shows further division into core and halo regions. The core is defined as the inner region whose potential is above ε_F, while the halo is defined as the inner region whose potential is below ε_F plus the outer region whose potential is between ε_h and ε_s; (c) shows isopotentials of the stream function, including the separatrix ε_s and the Fermi energy ε_F. The uncolored region marks all outer isopotentials with energy greater than the halo energy ε_h – the separatrix of the initial condition.

total energy inside the system is conserved. The updates in (4.19) will end when the distribution converges to the final stationary state with energy $E = E_0$. Note that the total energy is computed in the laboratory frame. This is necessary because the rotational velocity changes with each iteration, until a stationary state is reached.

The different stages of SCHA are shown in Figure 13. It shows the distribution function overlaid by the isopotential levels of the stream function as the calculation progresses. The vortices move from the *inactive* regions to the core and halo regions, according to the established rules. Starting from a continuous vortex distribution, SCHA converges to a highly non-trivial distribution function that rotates in the laboratory frame with constant

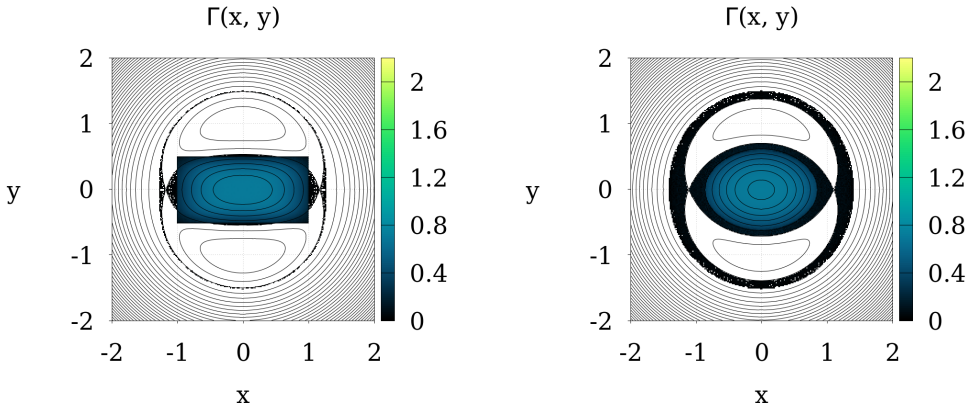

Figure 13 – Subsequent stages of SCHA corresponding to the evolution of the distribution function in in Figure 10 with the contour plot of its potential overlaid over the phase space snapshots obtained from SCHA. Note that the vortices move from *inactive* regions according to the established criteria for core and halo regions.

angular velocity and has a high-density elliptical core surrounded by a low-density halo, see Figure 13. In Figures 14 to 23, more complex continuous initial distributions are considered, the resulting steady-state (in the rotating frame) density profiles are compared with the results of molecular dynamics simulations.

A flaw in this core-halo approach is that the maximum extent of the halo is calculated from the separatrix of the initial vortex distribution function. If such a distribution function is linearly unstable, which is the case at high aspect ratios, the resulting instability can expel vortices beyond the extent of the separatrix [23]. Figures 14, 16, 18, and 20 show the stationary solutions (in rotating frame) compared with MD simulations for various initial distributions. One can see that for these initial distributions the halos extend farther than what is predicted by the theory. Nevertheless, since the halo density is so small, this has only a very minor effect on the density distribution and the shape of the core region, which are very accurately described by the core-halo theory. For a more quantitative comparison of the theory with the simulations, Figures 15, 17, 19, and 21 present the vortex density distributions along the principal axes, showing that the theory accounts for the density distribution in the core quantitatively and in the halo semi-quantitatively. What is even more impressive is that the theory predicts that one-level rectangular distribution with an aspect ratio greater than ~ 6.3 relaxes into two identical distorted elliptical vortex patches of complex shape surrounded by a halo and rotating about their center of mass. This is quantitatively verified by MD simulations, which show that splitting into two identical vortex patches occurs at aspect ratios of ~ 6.1 or greater. Figures 22 and 23 compare the steady-state from SCHA and MD simulations for an aspect ratio of 6.5. They show excellent agreement.

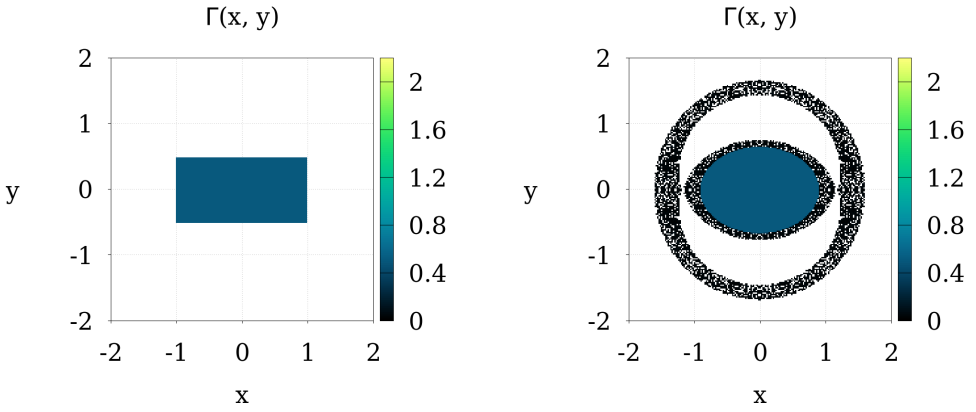

(a) Initial condition

(b) SCHA's steady-state

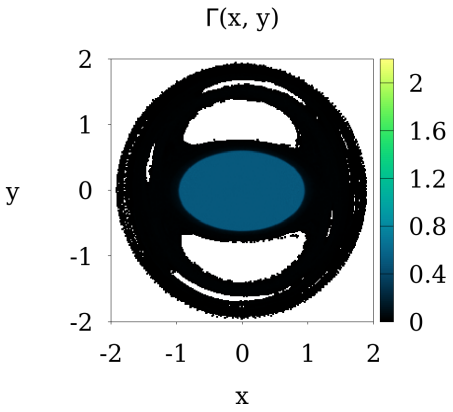

(c) MD simulation's steady-state

Figure 14 – Snapshots of the phase space obtained using the SCHA and MD simulation. The initial condition is a one-level rectangular distribution function, $f(x, y) = 0.5\,\Theta\,(1.0 - |x|)\;\Theta\,(0.5 - |y|)$, normalized to unity. The MD simulation has halo that extends farther than predicted by the theory.

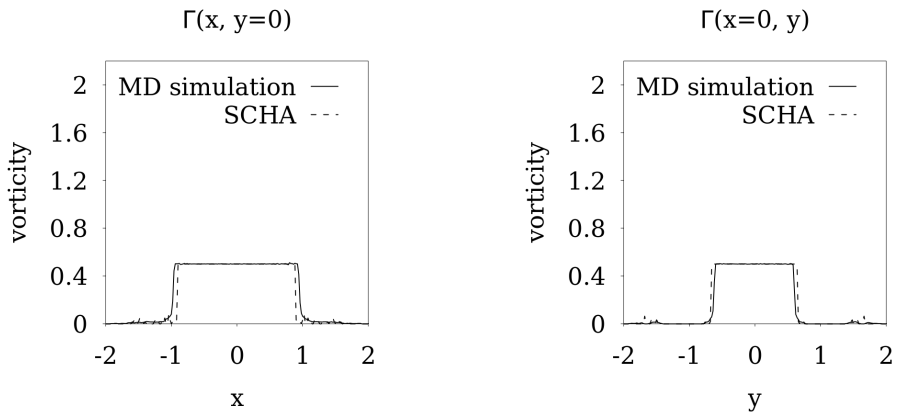

Figure 15 – Comparison of the density distribution over the x- and y-axis of the steady-states obtained using the SCHA and MD simulation. These correspond to the steady states shown in Figure 14.

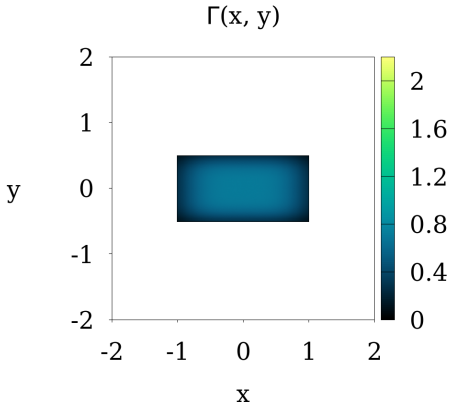

(a) Initial condition

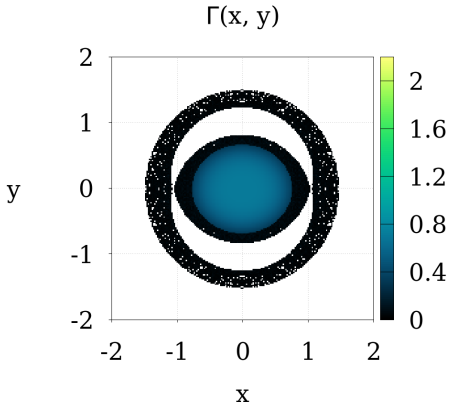

(b) SCHA's steady-state

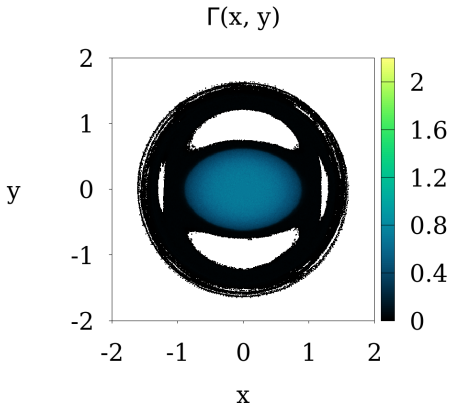

(c) MD simulation's steady-state

Figure 16 – Snapshots of the phase space obtained using the SCHA and MD simulation. The initial condition is a continuous rectangular distribution function, $f(x, y) = 0.7\,\mathrm{e}^{-x^4-16y^4}\,\Theta\,(1.0 - |x|)\,\Theta\,(0.5 - |y|)$, normalized to unity.

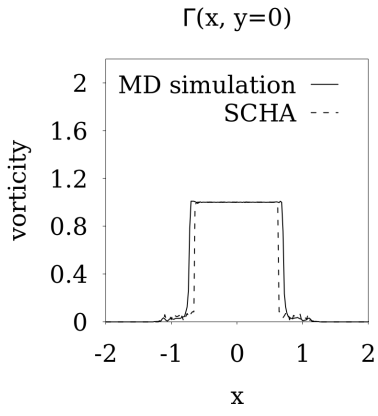

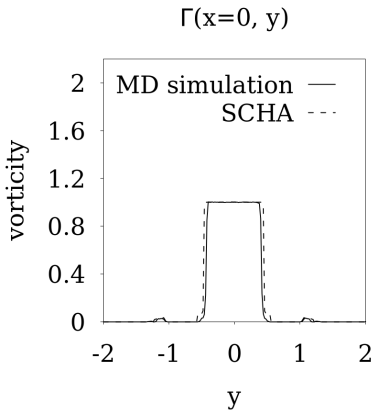

Figure 17 – Comparison of the density distribution over the x- and y-axis of the steady-states obtained using the SCHA and MD simulation. These correspond to the steady states shown in Figure 16.

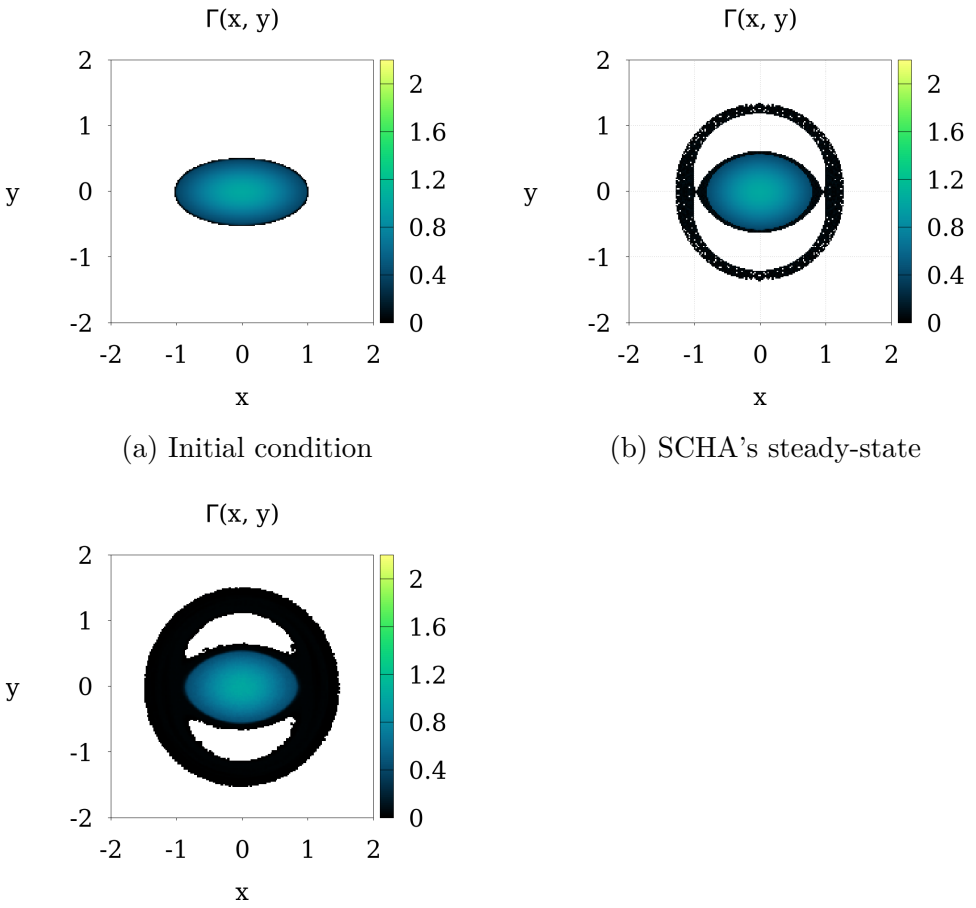

(a) Initial condition

(b) SCHA's steady-state

(c) MD simulation's steady-state

Figure 18 – Snapshots of the phase space obtained using the SCHA and MD simulation. The initial condition is a continuous elliptical distribution function, $f(x, y) = 1.0\, e^{-x^2-4y^2}\, \Theta\,(1.0 - x^2 - 4y^2)$, normalized to unity.

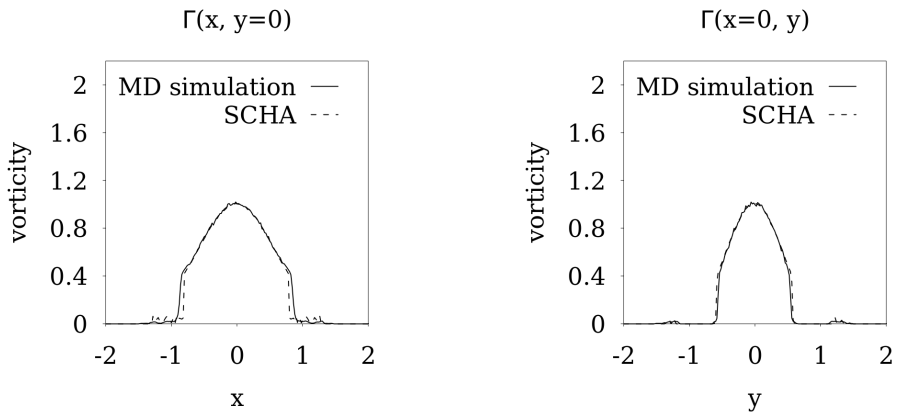

Figure 19 – Comparison of the density distribution over the x- and y-axis of the steady-states obtained using the SCHA and MD simulation. These correspond to the steady states shown in Figure 18.

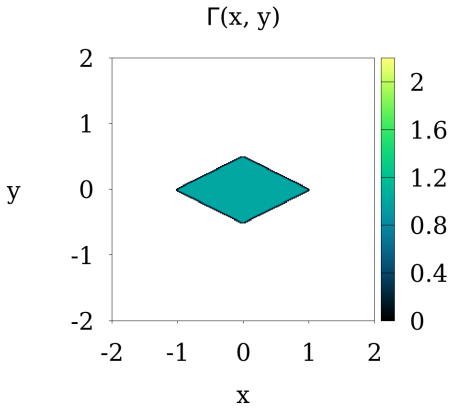

(a) Initial condition

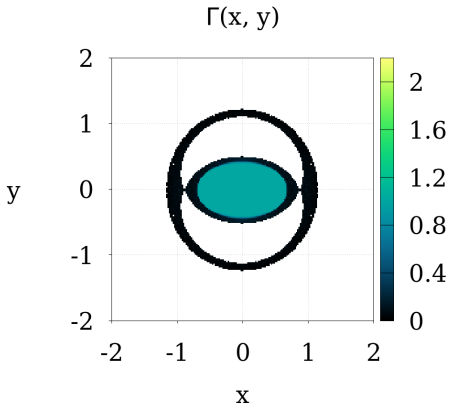

(b) SCHA's steady-state

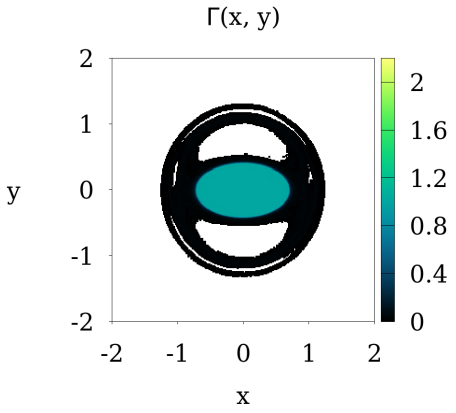

(c) MD simulation steady-state

Figure 20 – Snapshots of the phase space obtained using the SCHA and MD simulations. The initial condition is a one-level rhombic distribution function, $f(x, y) = \Theta\left(1.0 - |x| - 2|y|\right)$, normalized to unity. As in the other simulations, the MD simulation exhibit a thicker halo, but the core predicted by the SCHA is very similar to the core observed in the MD simulation.

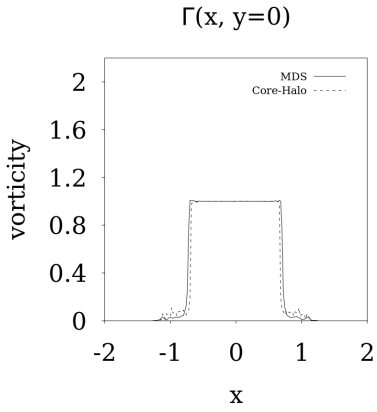

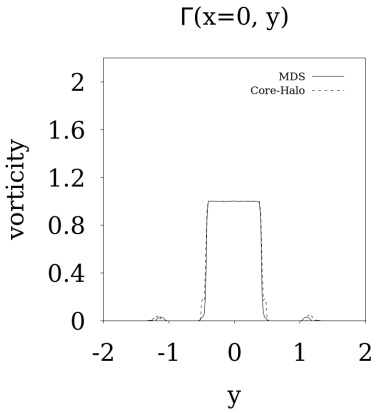

Figure 21 – Comparison of the vortex density distribution along the x- and y-axis in the steady-state predicted using the SCHA and compared with MD simulations. These correspond to the steady state shown in Figure 20.

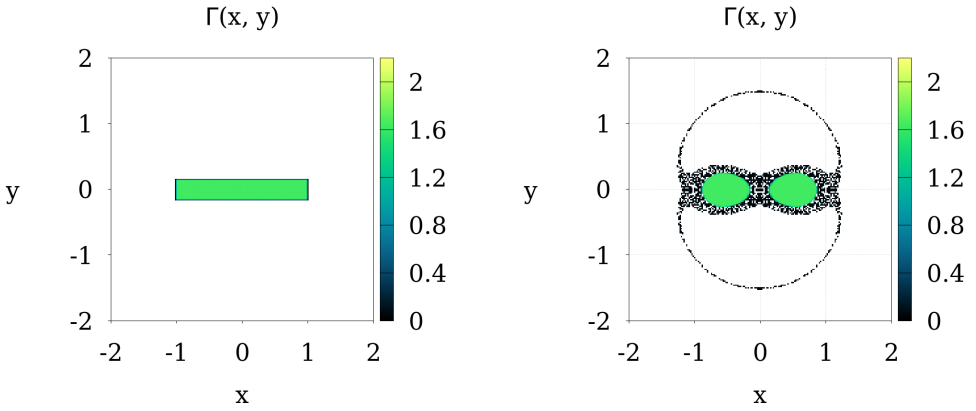

(a) Initial condition

(b) SCHA's steady-state

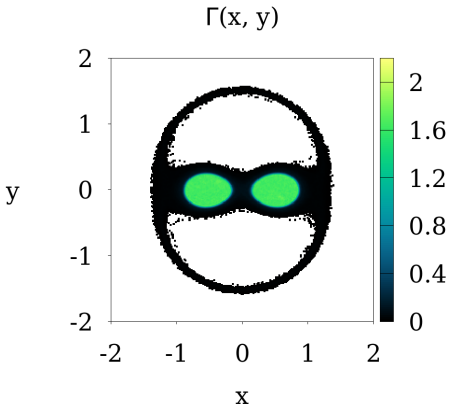

(c) MD simulation steady-state

Figure 22 – Snapshots of the phase space obtained using the SCHA and MD simulation. The initial condition is a one-level rectangular distribution function, $f(x, y) = 1.625\,\Theta\,(1.0 - |x|)\;\Theta\,(1/6.5 - |y|)$. As in the other simulations, the MD simulation exhibit a thicker halo.

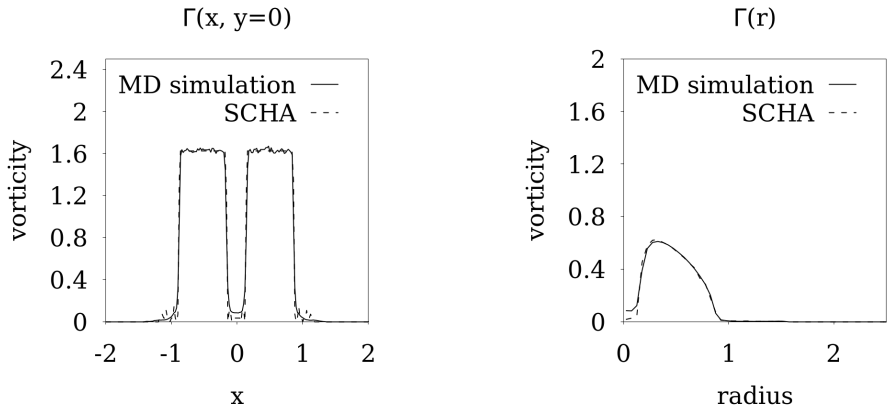

Figure 23 – Comparison of the density distribution over the x-axis and radial distribution of the steady-states obtained using the SCHA and MD simulation. These correspond to the steady states shown in Figure 22. The radial distribution is defined as $\Gamma(r) = (2\pi)^{-1} \int_0^{2\pi} \Gamma(r, \theta) \mathrm{d}\theta$.

Part III

Final Considerations

5 Conclusion

Systems with long-range interactions have peculiarities in their dynamical and equilibrium properties compared to systems with short-range interactions. Typically, the methods of classical statistical mechanics do not work for systems with long-range interactions, where dynamical aspects must be taken into account. From a dynamical point of view, the dominance of the mean field leads to a collisionless relaxation process, which results in longstanding quasi-stationary states that do not exhibit a Maxwell-Boltzmann velocity distribution. The quasi-stationary states correspond to stationary solutions of the Vlasov dynamics, which is valid only in the limit $N \to \infty$. For systems of finite size, however, the Vlasov dynamics is only a zero-order approximation. The kinetic equations resulting from the quasi-linear first-order approximations are the Landau and Lenard-Balescu equations, where finite-size effects drive the system towards equilibrium on a characteristic time scale $\tau \propto N^{\delta}$, where δ is usually larger than one. Nevertheless, even at equilibrium, properties such as inequivalence of ensembles can be observed near phase transitions because the additive property is not present.

This is not the case in two-dimensional fluid dynamics, since single vortices with finite strength are physically impossible. Therefore, the Euler equation can only be mapped to a system of infinite point-like vortices, which means that a stationary Vlasov state is actually the final stage of evolution. The work developed in this thesis takes advantage of this property and relies on statistical approaches of the single-particle distribution function. In particular, Kirchhoff's vortex formalism is used to study stationary solutions of the two-dimensional Euler equations, where the vortex dynamics obeys Hamilton's equations of motion, and the x and y coordinates of the vortex position form a conjugate pair. A two-dimensional fluid state can therefore be expressed by an infinite number of infinitesimal vortices. The Hamiltonian structure of the vortex dynamics naturally draws an analogy with short-range interacting systems. Specifically, it's known that the equilibrium state to which a many-body system – such as a gas or a colloidal suspension – will evolve from an arbitrary initial distribution can be calculated using molecular dynamics simulations. On the other hand, Boltzmann-Gibbs statistical mechanics allows to predict the final thermodynamic equilibrium with no need to perform molecular dynamics simulations. In practice, it's often impossible to calculate the partition function except for very simple systems. Alternatively, one can use Monte Carlo simulations to obtain the equilibrium state of a system, which simply put is just a statistical tool to perform entropy maximization numerically. The difficulty is that for systems with long-range interactions – such as vortices in Euler's fluid, gravitational systems, or magnetically confined plasmas – one cannot use Boltzmann-Gibbs statistical mechanics. As stated, these systems do not evolve to thermodynamic equilibrium, but are stuck in non-equilibrium steady states.

Under these conditions, the Vlasov equation governs the dynamics, so Lynden-Bell relaxation theory can be applied to study how different vortex fields relax to steady states in a rotating reference frame.

In this way, a stochastic method is presented which allows to easily obtain the state of maximum entropy starting from an arbitrary initial distribution, preserving all Casimir invariants of the system. The results are compared with the equilibrium states found using molecular dynamics simulations – and qualitatively with the Onsager model for point-like vortices. Via molecular dynamics simulations, an equilibrium state corresponding to the maximum entropy of Boltzmann-Gibbs statistical mechanics is not reached. The final state to which the fluid evolves is indeed very different from that of maximum entropy, from which one can infer that no mixing takes place in the vortex dynamics.

Both Onsager's theory and Lynden-Bell's maximum entropy principle rely on the ergodicity hypothesis, which, however, cannot be considered due to the lack of additivity. The core-halo theory is then presented, which allows a semi-quantitative prediction of the final state to which the vortex fluid will relax. In particular, the vortex distribution is stationary only in a rotating reference frame, while in the laboratory frame it has a very complex, non-axisymmetric form, rotating with constant angular velocity – which the theory allows us to calculate explicitly. If the initial vortex distribution has a large aspect ratio, it divides at steady state into two distorted elliptical vortex patches rotating about their center of mass and surrounded by a tenuous halo. The theory allows us to accurately predict the bifurcation point and the final stationary vortex distribution.

Bibliography

[1] Karsten Ahnert and Mario Mulansky. Odeint – solving ordinary differential equations in C++. *AIP Conference Proceedings*, 1389(1):1586–1589, 2011. Cited 2 times on pages 47 and 49.

[2] Angel Alastuey, Marc Magro, and Pierre Pujol. *Physique et outils mathématiques: méthodes et exemples*. L'Editeur : EDP Sciences, 2008. Cited on page 39.

[3] I. Arad and D. Lynden-Bell. Inconsistency in theories of violent relaxation. *Monthly Notices of the Royal Astronomical Society*, 361(2):385–395, August 2005. Cited on page 16.

[4] V I Arnold and Boris A Khesin. *Topological methods in hydrodynamics*. Applied mathematical sciences. Springer, New York, NY, December 1998. Cited on page 9.

[5] Julien Barré, David Mukamel, and Stefano Ruffo. Inequivalence of ensembles in a system with long-range interactions. *Phys. Rev. Lett.*, 87:030601, Jun 2001. Cited 2 times on pages 16 and 26.

[6] Richard Barrett, Michael Berry, Tony F. Chan, James Demmel, June Donato, et al. *Templates for the Solution of Linear Systems: Building Blocks for Iterative Methods*. Society for Industrial and Applied Mathematics, January 1994. Cited on page 49.

[7] D. Bindoni and L. Secco. Violent relaxation in phase-space. *New Astronomy Reviews*, 52(1):1–18, May 2008. Cited on page 16.

[8] James Binney and Scott Tremaine. *Galactic dynamics*. Princeton Series in Astrophysics. Princeton University Press, 2 edition, January 2008. Cited on page 17.

[9] F. Bouchet and J. Barré. Classification of phase transitions and ensemble inequivalence, in systems with long range interactions. *Journal of Statistical Physics*, 118 (5-6):1073–1105, mar 2005. Cited on page 16.

[10] W. Braun and K. Hepp. The vlasov dynamics and its fluctuations in the 1/n limit of interacting classical particles. *Communications in Mathematical Physics*, 56(2): 101–113, jun 1977. Cited on page 24.

[11] Jacob Burbea and Michael Landau. The kelvin waves in vortex dynamics and their stability. *Journal of Computational Physics*, 45(1):127–156, 1982. ISSN 0021-9991. Cited 2 times on pages 49 and 50.

[12] Herbert B Callen. *Thermodynamics and an Introduction to Thermostatistics*. John Wiley & Sons, 2 edition, August 1985. Cited 2 times on pages 15 and 24.

[13] A. Campa, T. Dauxois, D. Fanelli, and S. Ruffo. *Physics of Long-Range Interacting Systems*. Oxford University Press, 08 2014. ISBN 9780199581931. Cited on page 46.

[14] Alessandro Campa, Thierry Dauxois, and Stefano Ruffo. Statistical mechanics and dynamics of solvable models with long-range interactions. *Physics Reports*, 480(3): 57–159, 2009. ISSN 0370-1573. Cited 4 times on pages 15, 16, 19, and 25.

[15] Alessandro Campa, Thierry Dauxois, and Stefano Ruffo. Statistical mechanics and dynamics of solvable models with long-range interactions. *Physics Reports*, 480(3): 57–159, 2009. ISSN 0370-1573. Cited on page 46.

[16] Shiyi Chen, Robert Ecke, Gregory Eyink, Michael Rivera, Minping Wan, et al. Physical mechanism of the two-dimensional inverse energy cascade. *Physical review letters*, 96:084502, 04 2006. Cited on page 17.

[17] J. P. Christiansen and N. J. Zabusky. Instability, coalescence and fission of finite-area vortex structures. *Journal of Fluid Mechanics*, 61(2):219–243, 1973. Cited on page 47.

[18] O Cohen and D Mukamel. Ensemble inequivalence: Landau theory and the abc model. *Journal of Statistical Mechanics: Theory and Experiment*, 2012(12):P12017, dec 2012. Cited on page 16.

[19] Thierry Dauxois, Stefano Ruffo, and Leticia F Cugliandolo. *Long-range interacting systems*. École d'été de Physique des Houches. Oxford University Press, November 2009. Cited on page 19.

[20] D. G. Dritschel, R. K. Scott, C. Macaskill, G. A. Gottwald, and C. V. Tran. Unifying scaling theory for vortex dynamics in two-dimensional turbulence. *Phys. Rev. Lett.*, 101:094501, Aug 2008. Cited on page 47.

[21] David G. Dritschel, Richard K. Scott, Charlie Macaskill, Georg A. Gottwald, and Chuong V. Tran. Late time evolution of unforced inviscid two-dimensional turbulence. *Journal of Fluid Mechanics*, 640:215–233, 2009. Cited on page 47.

[22] Gregory L. Eyink and Katepalli R. Sreenivasan. Onsager and the theory of hydrodynamic turbulence. *Rev. Mod. Phys.*, 78:87–135, Jan 2006. Cited on page 46.

[23] Calvin A Fracassi Farias, Renato Pakter, and Yan Levin. Linear and non-linear instabilities of kirchhoff's elliptical vortices. *Journal of Statistical Mechanics: Theory and Experiment*, 2020(8):083205, aug 2020. Cited 2 times on pages 50 and 56.

[24] A. Figueiredo, T. M. Rocha Filho, M. A. Amato, Z. T. Oliveira, and R. Matsushita. Truncated lévy flights and weak ergodicity breaking in the hamiltonian mean-field model. *Phys. Rev. E*, 89:022106, Feb 2014. Cited on page 16.

[25] T M Rocha Filho. Non-equilibrium entropy and dynamics in a system with long-range interactions. *Journal of Physics A: Mathematical and Theoretical*, 49(18): 185002, March 2016. Cited on page 18.

[26] T. M. Rocha Filho, A. Figueiredo, and M A. Amato. Entropy of classical systems with long-range interactions. *Phys. Rev. Lett.*, 95:190601, Nov 2005. Cited on page 16.

[27] A. Hadjidimos. Successive overrelaxation (sor) and related methods. *Journal of Computational and Applied Mathematics*, 123(1):177–199, 2000. ISSN 0377-0427. Cited on page 48.

[28] H Helmholtz. LXIII. On Integrals of the hydrodynamical equations, which express vortex-motion. *London, Edinburgh, Dublin Philos. Mag. J. Sci.*, 33(226):485–512, 1867. Cited on page 45.

[29] Kerson Huang. *Statistical Mechanics*. John Wiley & Sons, 2 edition, April 1987. Cited 2 times on pages 15 and 37.

[30] Gustav Kirchhoff. *Vorlesungen über mathematische Physik. Mechanik*, volume 1. Teubner, 1876. Cited on page 18.

[31] Piotr Kubala, Piotr Sierant, Giovanna Morigi, and Jakub Zakrzewski. Ergodicity breaking with long-range cavity-induced quasiperiodic interactions. *Phys. Rev. B*, 103:174208, May 2021. Cited on page 16.

[32] A. Lederhendler and D. Mukamel. Long-range correlations and ensemble inequivalence in a generalized *abc* model. *Phys. Rev. Lett.*, 105:150602, Oct 2010. Cited on page 16.

[33] Yan Levin, Renato Pakter, and Felipe B. Rizzato. Collisionless relaxation in gravitational systems: From violent relaxation to gravothermal collapse. *Phys. Rev. E*, 78:021130, Aug 2008. Cited on page 37.

[34] Yan Levin, Renato Pakter, and Tarcisio N. Teles. Collisionless relaxation in non-neutral plasmas. *Phys. Rev. Lett.*, 100:040604, Jan 2008. Cited on page 37.

[35] Yan Levin, Renato Pakter, Felipe B. Rizzato, Tarcísio N. Teles, and Fernanda P.C. Benetti. Nonequilibrium statistical mechanics of systems with long-range interactions. *Physics Reports*, 535(1):1–60, 2014. ISSN 0370-1573. Cited 2 times on pages 19 and 46.

[36] A. E. H. Love. On the Stability of certain Vortex Motions. *Proceedings of the London Mathematical Society*, s1-25(1):18–43, 11 1893. ISSN 0024-6115. Cited on page 49.

[37] D. Lynden-Bell. Statistical Mechanics of Violent Relaxation in Stellar Systems. *Monthly Notices of the Royal Astronomical Society*, 136(1):101–121, 05 1967. ISSN 0035-8711. Cited 2 times on pages 16 and 35.

[38] D. Lynden-Bell. Negative specific heat in astronomy, physics and chemistry. *Physica A: Statistical Mechanics and its Applications*, 263(1):293–304, 1999. ISSN 0378-4371. Cited on page 16.

[39] Carlo Marchioro and Mario Pulvirenti. *Mathematical Theory of Incompressible Nonviscous Fluids*. Springer New York, 1994. Cited 2 times on pages 9 and 46.

[40] Julien Michel and Raoul Robert. Statistical mechanical theory of the great red spot of jupiter. *Journal of Statistical Physics*, 77(3-4):645–666, November 1994. Cited on page 17.

[41] T. B. Mitchell and L. F. Rossi. The evolution of kirchhoff elliptic vortices. *Physics of Fluids*, 20(5):054103-054103-12, may 2008. Cited on page 50.

[42] Luis G. Moyano and Celia Anteneodo. Diffusive anomalies in a long-range hamiltonian system. *Phys. Rev. E*, 74:021118, Aug 2006. Cited on page 17.

[43] Tadas K. Nakamura. Statistical mechanics of a collisionless system based on the maximum entropy principle. *The Astrophysical Journal*, 531(2):739–743, March 2000. Cited on page 16.

[44] Norihiko Nakauchi, Hiroshi Oshima, and Yoshio Saito. Inverse energy cascade in a nearly two-dimensional turbulence. *Physics of Fluids A: Fluid Dynamics*, 2(3): 435–442, March 1990. Cited on page 17.

[45] Paul K Newton. *The N-Vortex Problem*. Applied Mathematical Sciences. Springer, New York, NY, December 2010. Cited on page 9.

[46] L. Onsager. Statistical hydrodynamics. *Il Nuovo Cimento (1943-1954)*, 6(2):279–287, Mar 1949. ISSN 1827-6121. Cited 2 times on pages 17 and 45.

[47] Renato Pakter and Yan Levin. Nonequilibrium statistical mechanics of two-dimensional vortices. *Phys. Rev. Lett.*, 121:020602, Jul 2018. Cited 2 times on pages 18 and 49.

[48] Renato Pakter, Bruno Marcos, and Yan Levin. Symmetry breaking in d-dimensional self-gravitating systems. *Phys. Rev. Lett.*, 111:230603, Dec 2013. Cited on page 16.

[49] Linda E Reichl. *A modern course in statistical physics*. Wiley-VCH Verlag, 4 edition, April 2016. Cited 2 times on pages 15 and 24.

[50] David Ruelle. *Statistical mechanics: Rigorous results*. W.A. Benjamin, 1969. Cited 2 times on pages 16 and 25.

[51] G. W. S. Templates for the solution of linear systems: Building blocks for iterative methods. *Mathematics of Computation*, 64(211):1349–1352, 1995. ISSN 00255718, 10886842. Cited on page 42.

[52] Tarcísio N. Teles, Fernanda P. da C. Benetti, Renato Pakter, and Yan Levin. Nonequilibrium phase transitions in systems with long-range interactions. *Phys. Rev. Lett.*, 109:230601, Dec 2012. Cited on page 26.

[53] W. Thirring. Systems with negative specific heat. *Zeitschrift für Physik A Hadrons and nuclei*, 235(4):339–352, aug 1970. Cited on page 16.

[54] Sir William Thomson. Xxiv. vibrations of a columnar vortex. *The London, Edinburgh, and Dublin Philosophical Magazine and Journal of Science*, 10(61):155–168, 1880. Cited on page 50.

[55] Shuling Tian, Yisheng Gao, Xiangrui Dong, and Chaoqun Liu. Definitions of vortex vector and vortex. *Journal of Fluid Mechanics*, 849:312–339, June 2018. Cited on page 45.

[56] Yoshiyuki Y. Yamaguchi, Julien Barré, Freddy Bouchet, Thierry Dauxois, and Stefano Ruffo. Stability criteria of the vlasov equation and quasi-stationary states of the hmf model. *Physica A: Statistical Mechanics and its Applications*, 337(1):36–66, 2004. ISSN 0378-4371. Cited 2 times on pages 16 and 17.